HIGH ELECTRIC FIELD BEHAVIOR OF NEGATIVE IONS IN SUPERFLUID HELIUM

A THESIS

Presented to

The Faculty of the Division of Graduate

Studies and Research

by

Yu Liu

In Partial Fulfillment

of the Requirements for the Degree

Doctor of Philosophy

in the School of Physics

Georgia Institute of Technology

May, 1974

HIGH ELECTRIC FIELD BEHAVIOR OF NEGATIVE IONS

IN SUPERFLUID HELIUM

Approved:

Dr. Roger E. Little, Chairman

Dr. D. C. O'Shea

Dr. D. C. Ray

Date approved by Chairman: MAY 20, 1974

This thesis is gratefully

dedicated

to my parents

Mr. and Mrs. W. K. Liu

TABLE OF CONTENTS

ACKNOWLEDGMENTS

The author wishes to express his gratitude to the following persons:

To his thesis advisor, Dr. Roger E. Little, for his guidance, encouragement and teaching throughout this research.

To his thesis reading committee, Dr. D. C. O'Shea and Dr. D. C. Ray, for their comments and suggestions.

To Dr. H. A. Gersch and Dr. T. C. Padmore for many fruitful discussions.

To Dr. T. C. Padmore for the use of his computer program on vortex ring dynamics.

To Prof. L. A. Woodward for making photomicrographs of the grids.

To Mr. Kelly Springfield and the Physics Shop at the Georgia Institute of Technology for the construction of the apparatus of this experiment.

To his wife, Theresa, for her constant patience and support during his graduate study.

LIST OF TABLES

LIST OF ILLUSTRATIONS

Figure Page

SUMMARY

Several years ago, it was discovered that the negative helium ion in liquid helium was able to travel macroscopic distances in a zero electric field after it had passed through a region of high electric field. This phenomenon has been named the "persistence" of the drift velocity of the ion. This persistence current (persistence ion complex) has been interpretated as an electron trapped in a circular, singly quantized vortex ring. The experiments of this thesis project have been designed to test the vortex ring interpretation of persistence current by making range and size measurements and to discover additional properties of the persistence ion complex.

The farthest distance a vortex ring will go in a field-free region is defined as the range of the vortex ring. Size and range are directly related, knowledge of one is equivalent to knowledge of the other. A size measurement consists of placing a grid with appropriate sized openings in the path of the ion beam, which is produced by applying d.c. voltages between a radioactive source (Americium - 241, 19 μCi) and a collector. A vibrating reed electrometer is connected to the collector to measure the currents.

The following conclusions have been reached as a result of this research:

1. The persistence ion complex is not an electron trapped in a circular, singly quantized vortex ring.

2. The size of the persistence ion complex is about 35 microns.

3. The persistence ion complex can be created while the ion is in the vortex ring state.

4. The persistence ion complex breaks up at a sufficiently high electric field.

CHAPTER I

INTRODUCTION

For some time, helium ions have been used to investigate the microscopic structure of superfluid liquid helium.[1,2,3] Such ions are produced by allowing a radioactive source to ionize liquid helium. A positive ion consists of a He_2^+ ion surrounded by a region of helium of increased density due to polarization forces.[4] A negative ion consists of a free electron trapped in a low density "hole" in the liquid helium.[5] Rayfield and Reif[6,7] were the first ones to observe that ions, positive and negative, might be accelerated by an electric field to create vortex rings at sufficiently low temperatures. The behavior of ions can be investigated by conventional current techniques.

Several important factors may influence the motion of the ions. They are, for example, the applied electric forces on the bare ion and on the ion-ring complex, the frictional forces on the bare ion and on the ion-ring complex, the probability that the ion can be trapped by a vortex ring and the probability that the ion will escape from the ion-ring complex. The influence of these factors varies with temperature and applied electric field. As an ion is accelerated in an applied electric field at low temperatures, its motion passes through several stages. The average drift velocity of an ion with respect to the applied electric field is shown in Figure 1. At low electric fields, the bare ion behaves as it would in a simple fluid, its average

drift velocity increases linearly with the applied electric field.[8] As the ion reaches a critical velocity v_{c1} at a critical electric field E_{c1}, the motion of the ion has a dramatic change. The average drift velocity v_d decreases precipitously as the applied electric field increases.[9,10] This behavior is due to the trapping of ions into vortex rings and the increase in the size of the ion-ring complex as the vortex ring gains energy from the applied electric field. If nothing else happened, the average drift velocity of the ion-ring complex would continue decreasing as the electric field increased, as shown by the dashed line in Figure 1. However, the decline of the average drift velocity slows down as the applied electric field is further increased. At the second critical electric field E_{c2}, the average drift velocity of the ion once more increases with the applied electric field.[11] Even though the ion-ring complex may be completely stable with respect to the average forces, there is a finite probability that the ion will escape from its ring due to thermal fluctuation.[12] The minimum and rise in the average drift velocity are due to the increase in the escape probability of the ion from the vortex ring as the electric field is increased. The enhanced escape rate prevents the vortex ring from reaching the low velocities which correspond to a large vortex ring. This leads to an increase in the average drift velocity. After its escape, the bare ion accelerates once more to a velocity near v_{c1} and is captured by a new ring which then commences growing toward its equilibrium radius.[13,14] This sequence of events can be repeated many times. The representative ion histories are

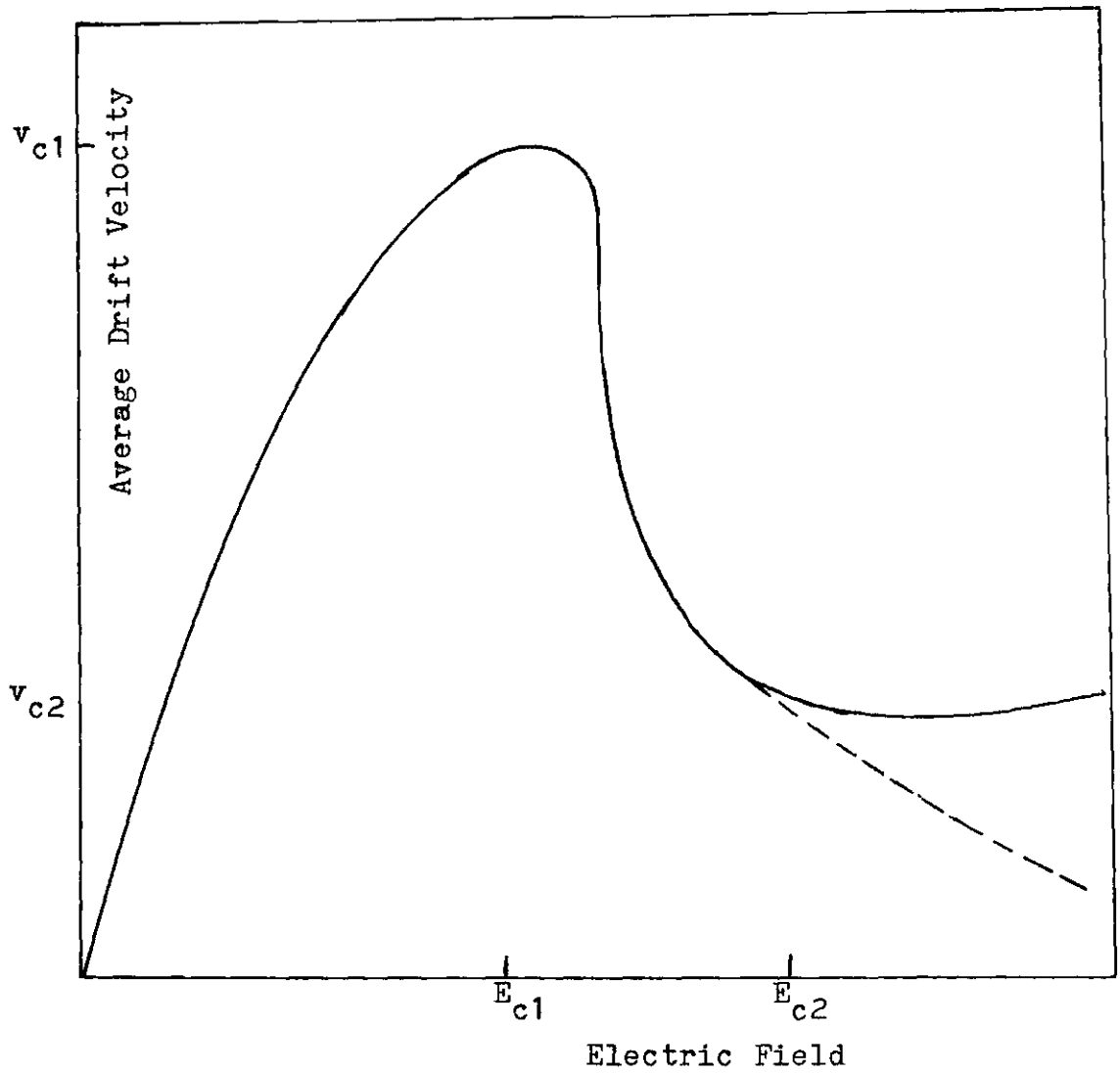

Figure 1. Average Drift Velocity of Ion vs Electric Field

illustrated in Figure 2. Curve (A) represents the ion velocity at an electric field smaller than the first critical field E_{c1}. It starts with an electric force larger than the frictional force acting on the ion. The ion velocity increases with time until it reaches a limiting value at which the frictional force equals the electric force. Curve (B) shows the ion velocity at an electric field between E_{c1} and E_{c2}. The ion velocity increases with time and then decreases with time due to the creation of a vortex ring, and finally reaches an equilibrium value. For electric fields higher than the second critical field E_{c2}, the early history of the ion velocity is similar to that of Curve (B). As time goes on, a second increase in the ion velocity occurs due to the escape of the ion from the vortex ring. As a second vortex ring is created, the ion velocity decreases again. This kind of process can repeat several times, hence more spikes can be observed on the ion velocity history at higher electric fields, as indicated in Curve (C). The dashed lines in Figure 2 show the average drift velocity of the ion at each electric field. Figure 2 is plotted using an arbitrary scale.

For temperatures below $1^{\circ}K$, the average drift velocity of the negative ion has a discontinuity at the first critical field. It is double-valued for fields just below the first critical field. After the ion has been accelerated to an electric field higher than the first critical field and a vortex ring has been created, the average drift velocity is then measured at fields smaller than the first critical field with the ion in the vortex ring state. These measured values are smaller than those measured at the same fields while the ion is still in the bare ion state. The positive ion behaves in a similar

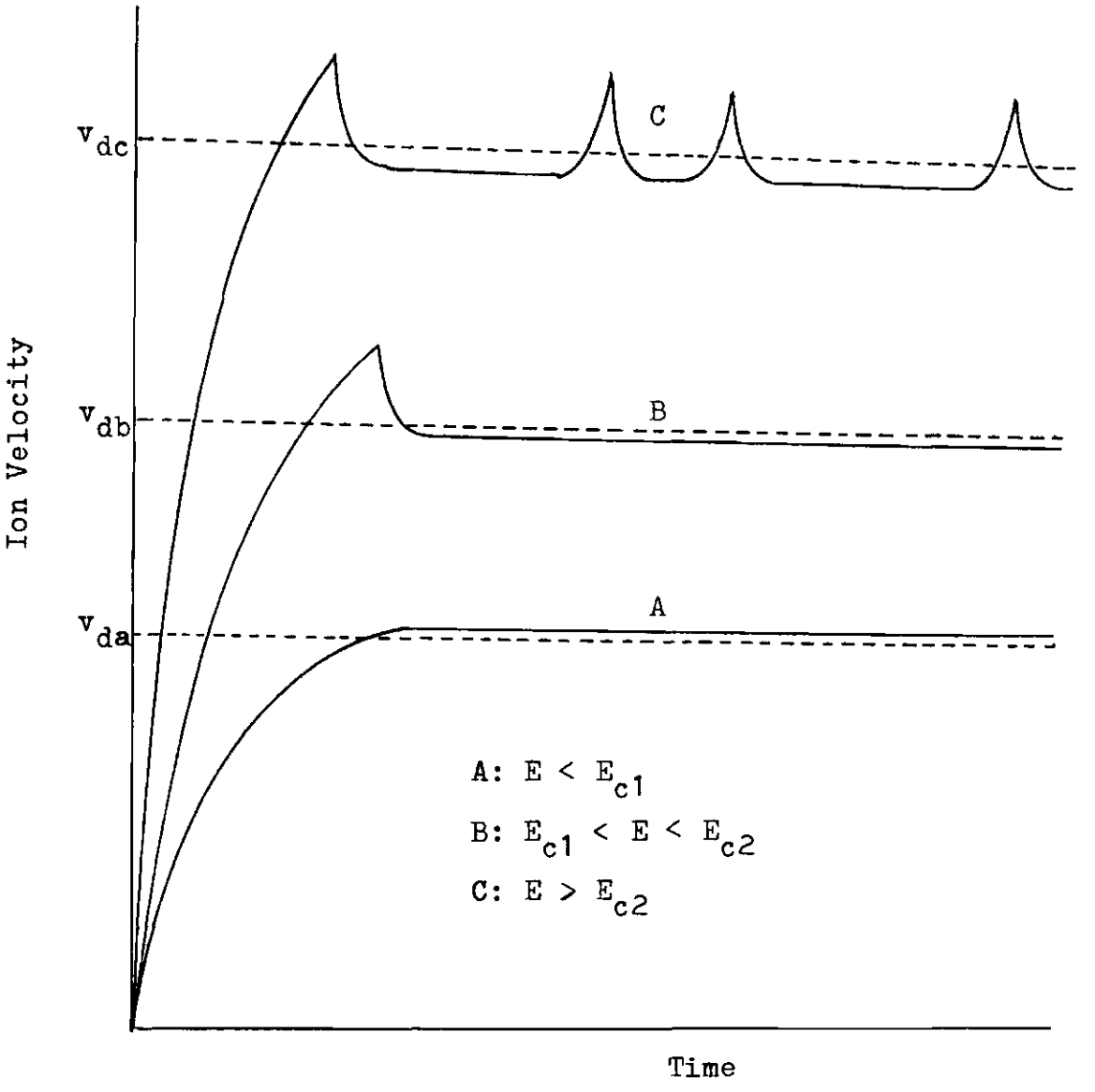

Figure 2. Ion Velocity vs Time

way at sufficiently low temperatures. In Figure 3, average drift velocities of both positive and negative ions at two temperatures are presented.

More detailed discussion of the behavior of ions in superfluid liquid helium is presented in the following sections.

Bare Ion

Ions are in the bare ion state immediately after they are emitted from the source. At low electric fields, the average drift velocity of the ion increases with the field. This behavior is similar to that of a particle moving in an ordinary viscous fluid. It can be assumed that the motion of the ion is governed by a balance between an electric field force eE and an average viscous frictional force f(v), where v is the instantaneous velocity of the ion. The equation of motion of the ion can be written as

$$M_{ion} \frac{dv}{dt} = eE - f(v). \qquad (1)$$

According to this picture, the ion accelerates from rest and approaches a limiting velocity at which the electric force and the frictional force are equal to each other.

Phonon and Roton

In 1941 Landau[15] suggested that the properties of superfluid liquid helium could be explained by describing the atomic motion of the liquid below the lambda point in terms of elementary excitations. These excitations are somewhat similar to the phonons in a crystal

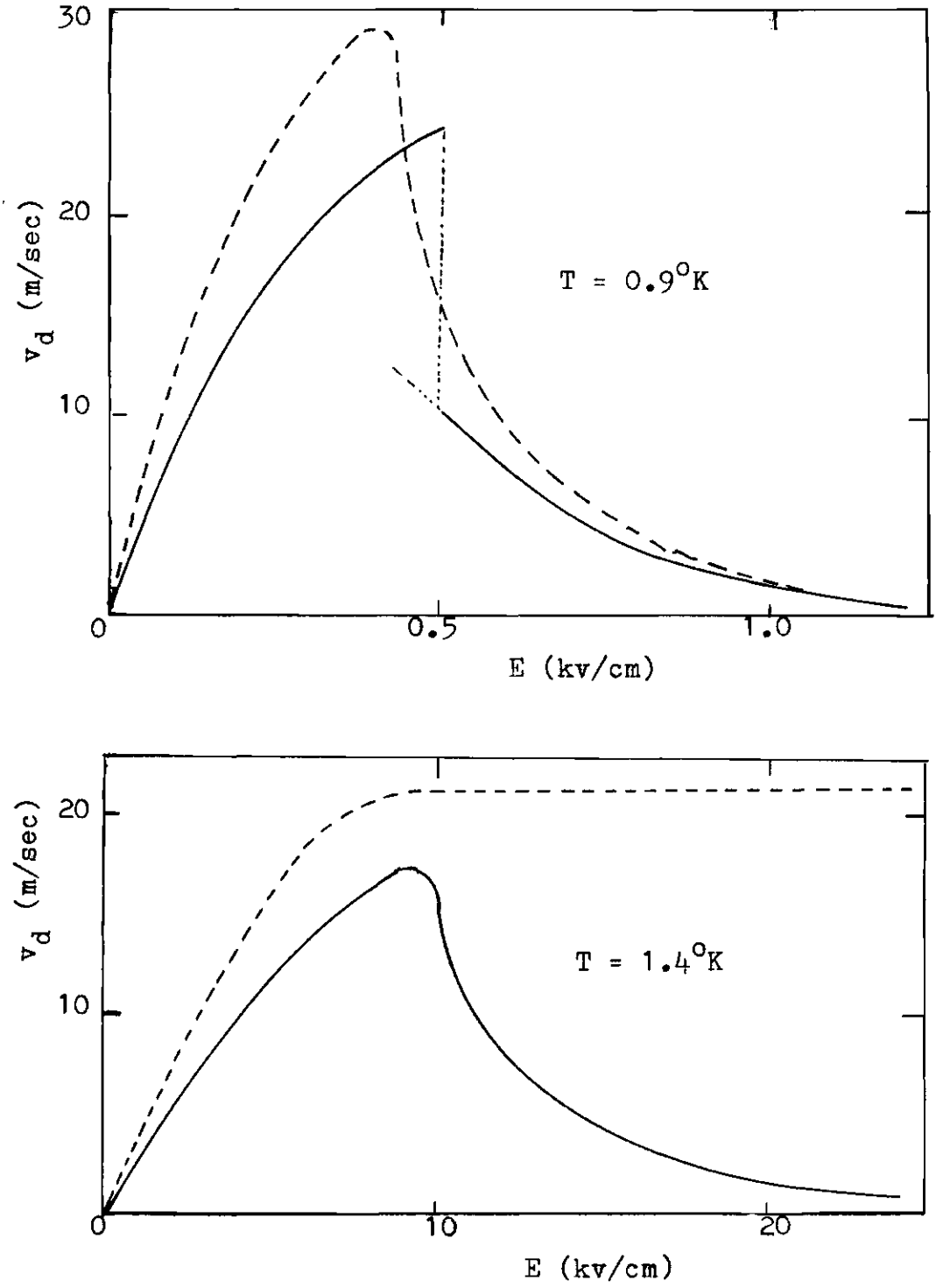

Figure 3. Drift Velocity of Positive and Negative Ions
Positive Ions: Dashed Lines
Negative Ions: Solid Lines

lattices. They are characterized by a frequency ω and a wavenumber k but have a different dispersion relation. Each excitation has a momentum $p = \hbar k$ and an energy $\epsilon = \hbar\omega$. The dispersion curve proposed by Landau[16] is illustrated in Figure 4. It turns out that most of the excitations have momenta in the regions of either the origin or the minimum. Landau specified the region near the origin by the phonon relation

$$\epsilon = cp$$

where c is the velocity of the longitudinal sound waves. The region of the minimum is specified by the relation

$$\epsilon = \Delta + \frac{(p-p_o)^2}{2\mu}$$

where Δ, p_o and μ are three constants derived from thermodynamic data. The excitations in this region are called "rotons". Phonons dominate at low temperatures. Rotons are more plentiful at $1^{\circ}K$. As an ion or a vortex ring moves in liquid helium, frictional forces are introduced as a result of its collisions with elementary excitations.

Vortex Ring

Donnelly and Roberts[17] suggested that a vortex ring is formed when a roton is expanded by thermal fluctuation to become a small ring. They assumed that proto-rings (rotons) are located near the equator of a moving ion. Collisions with other elementary excitations will occasionally make one of these proto-rings grow to finite size. The hydrodynamical attraction felt by an ion near the core of a vortex

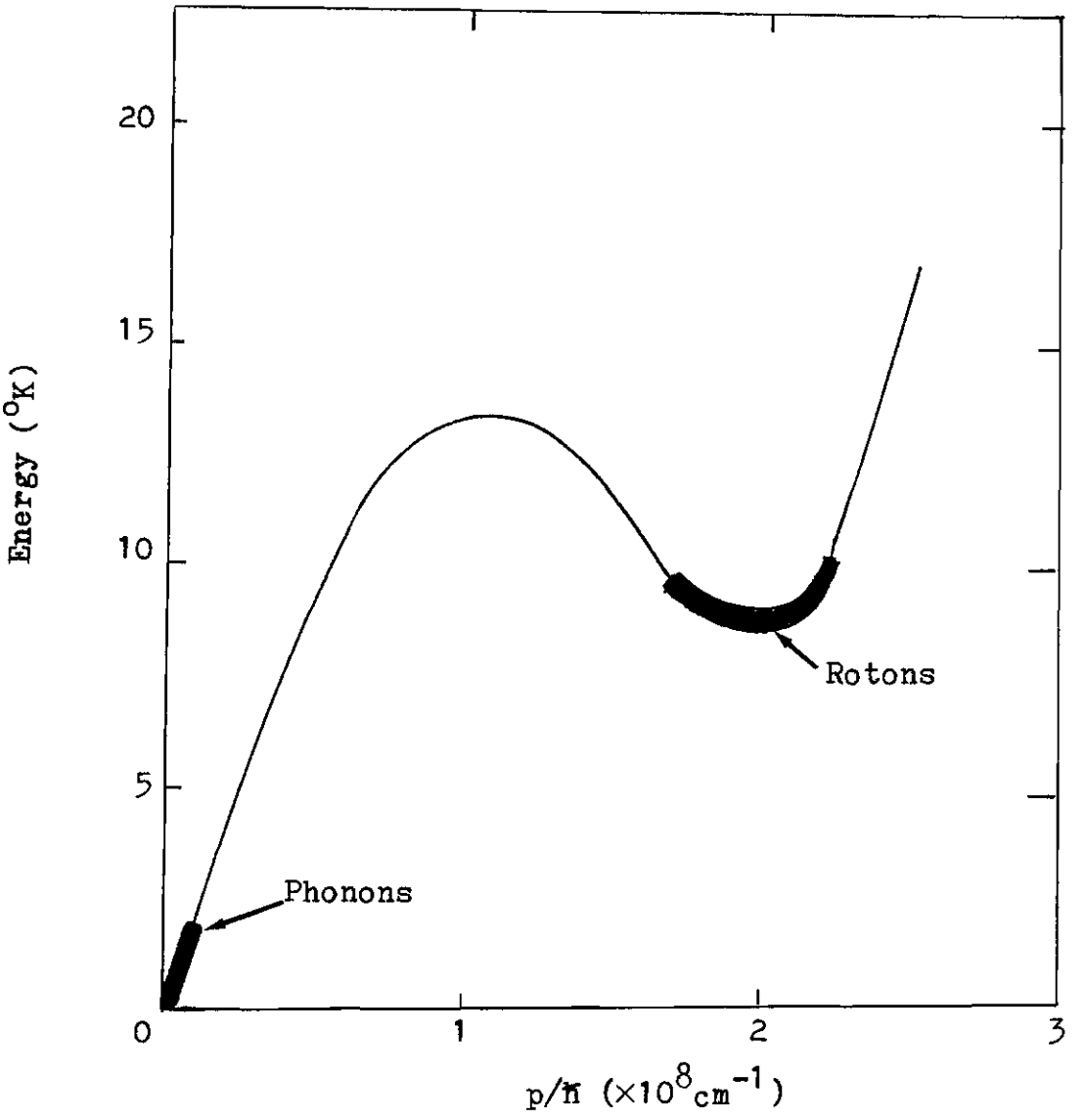

Figure 4. Elementary Excitations of the Landau Theory

will cause the ring to attach to the ion. When the ring grows to a size at which its forward velocity is equal to that of the ion, it is a "critical thermal fluctuation". Further growth of the ring will be at the expense of the external electric field, and will continue until the frictional force on the ring is equal and opposite to the electric force due to the external electric field.

Onsager[18] and Feynman[19] characterized the superfluid at absolute zero as a stationary rotational flow pattern with flow velocity u. In a quantum mechanical description, this flow pattern can be represented by a well-defined wavefunction $\Psi = \Psi_o \exp(iq)$ where Ψ_o is the ground state wavefunction of the fluid at rest and q is a phase factor whose gradient is related to the flow velocity u. The condition that Ψ be single-valued leads to the requirement that q changes by an integral multiple of 2π in going around any closed path. This requirement is equivalent to the Bohr-Sommerfeld condition in the form

$$\oint p \cdot dl = m \oint u \cdot dl = hN, \tag{2}$$

where p is the momentum associated with a helium atom of mass m moving with the flow velocity u, h is Planck's constant and N is an integer. The integral of the tangential velocity around a closed path is defined as the "circulation"

$$\kappa = \oint u \cdot dl. \tag{3}$$

In a cylindrical geometry, equation (3) reduces to $\kappa = 2\pi ru$, where r is the distance from the symmetry axis and u is the circumferential component of the flow velocity. Thus

$$u = \frac{\kappa}{2\pi r} \ . \qquad (4)$$

a relation characterizing the flow pattern of a vortex line. If r becomes less than some cut-off value a which is called the "core radius", u must deviate from equation (4) since it would otherwise become infinite.

As a further special case, let us consider the motion of two vortex lines of equal and opposite circulations, $\kappa_1 = -\kappa_2$. The distance between these two vortices is 2r as shown in Figure 5. This combination has been named "vortex-pair".[20] Vortex 1 produces a velocity $\kappa_1/2\pi(2r) = \kappa_1/4\pi r$ on vortex 2 at a right angle to the line joining them. In addition, vortex 2 induces a velocity $-\kappa_2/4\pi r$ on vortex 1, also at a right angle to r. Since $\kappa_1 = -\kappa_2$, the vortex-pair moves with constant velocity $\kappa/4\pi r$ at a right angle to the joining line.

A vortex ring, shown in Figure 6, has some similarity to a vortex-pair in that each element of the ring is influenced by the remaining elements and thus a velocity is given to the whole ring. The integration in this case is rather more involved. The velocity of a vortex ring was first given without proof by Thomson,[21] and was later verified by Hicks[22] and also by Gray.[23] It has since then been widely used in many hydrodynamics books as the velocity of a vortex ring in the form of

$$v = \frac{dx}{dt} = (\kappa/4\pi r)(\ln(8r/a) - \tfrac{1}{4}), \qquad (5)$$

where a is the core radius with a value of (1.28 ± 0.13) A, for a

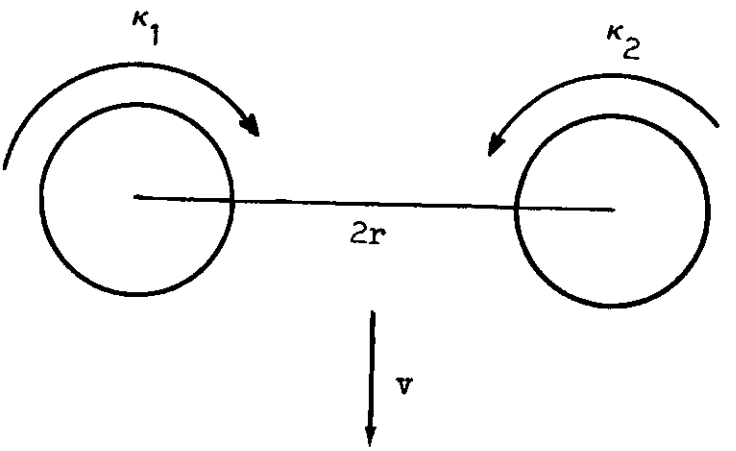

Figure 5. Vortex Pair

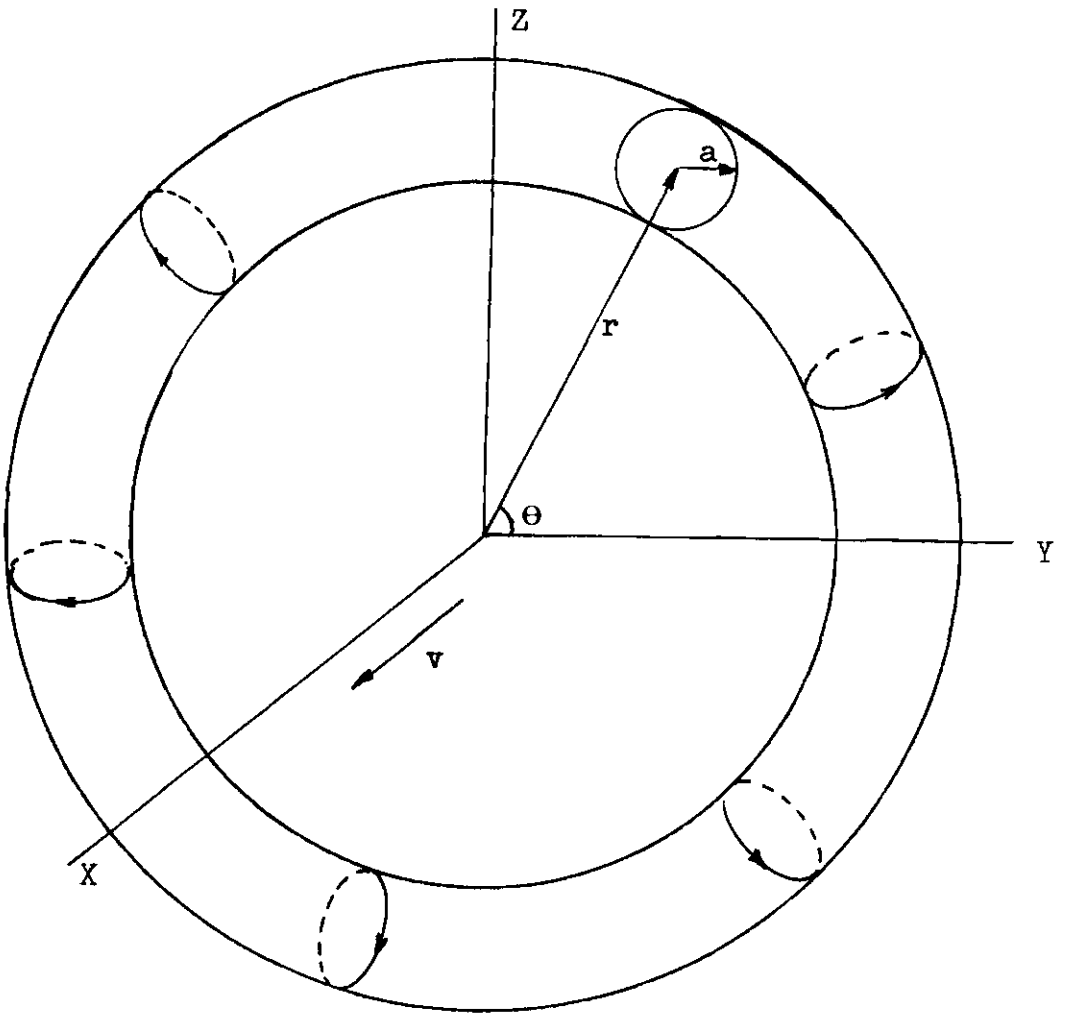

Figure 6. Vortex Ring Configuration

vortex ring in superfluid liquid helium,[7] and r is the radius of the vortex ring which is assumed much larger than a. The energy required to set the fluid into such motion from rest is given by

$$\epsilon = \tfrac{1}{2}\rho \iiint \left[v^2 + \left(\frac{dy}{dt}\right) + \left(\frac{dz}{dt}\right)^2\right] dxdydz, \tag{6}$$

where $y = r\sin\theta$, $z = r\cos\theta$ and ρ is the density of the fluid. Lamb carried out the detailed calculation of equation (6) in his book,[24] obtaining the result

$$\epsilon = \tfrac{1}{2}\rho\kappa^2 r(\ln(8r/a) - 7/4). \tag{7}$$

It is interesting to note from equations (5) and (7) that the radius of a vortex ring is approximately directly proportional to its energy, but inversely proportional to its velocity. This means that as a vortex ring moves in an electric field dominated region, it gains energy and its size grows, but its velocity decreases. On the other hand, as a vortex ring moves in a frictional force dominated region, it loses energy and its size reduces, but it moves faster.

In a similar fashion, Lamb calculated that the momentum of a vortex ring along the x-direction is equal to

$$p = \rho \iiint v dxdydz = \pi\rho\kappa r^2. \tag{8}$$

The total force acting on a vortex ring is the sum of an electric force eE and a frictional force f(v). According to Rayfield and Reif[7] the frictional force per unit length is proportional to its velocity, hence the frictional force on a vortex ring must be f(v) =

$C(2\pi r)v$. Then, the expression for v (equation (5)) shows that f(v) is a slowly varying function of the radius r, or energy ϵ, of the vortex ring. Rayfield and Reif also suggested that the frictional force is temperature dependent. More precisely, the frictional force can be written in the form

$$f(v) = - \alpha(T)(\ln(8r/a) - \tfrac{1}{4}).$$

Thus the total force acting on a vortex ring becomes

$$F = eE - \alpha(\ln(8r/a) - \tfrac{1}{4}). \qquad (9)$$

High Field Behavior

As indicated in Figure 1, the average drift velocity of an ion starts decreasing at the first critical field E_{c1} due to the formation of a vortex ring. The decline of the average drift velocity slows down and the drift velocity reaches a minimum at the second critical field E_{c2} due to the escape of the ion from the vortex ring.[13,14] After the escape the ion will be accelerated in the electric field to a velcoity close to v_{c1} and captured by a new ring. This sequence can be repeated many times.

Figure 7 shows the average drift velocities of positive ions at four different temperatures, measured by Bruschi, Mazzoldi and Santini.[11] The decline of the average drift velocity at the first critical field becomes less steep at higher temperatures. This means that escapes happen more frequently at higher temperatures. For the positive ion, the effect of escapes has been seen down to temperatures near $0.5^{\circ}K$.[25] At temperatures above $1^{\circ}K$, the effects of escapes are

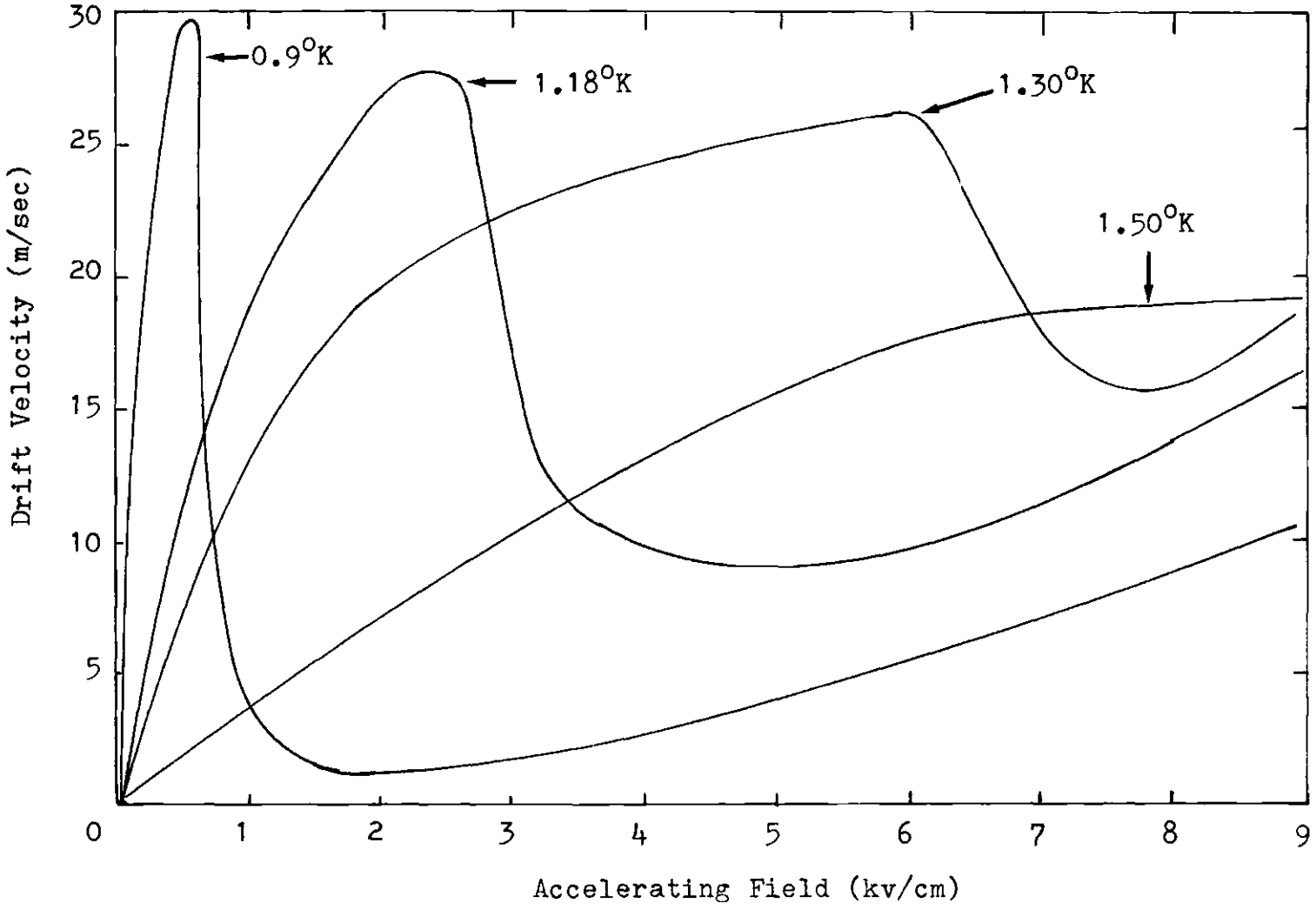

Figure 7. Drift Velocity of Positive Ion. (After Bruschi, Mazzoldi and Santini)

inevitable at all fields.[26] The negative ion is more strongly bound to the vortex ring. Its escape probability is significant only for electric fields larger than 20 kv/cm or temperatures higher than 1.5°K.[27] The decline of the average drift velocity of negative ions at the first critical field is clear even for temperatures up to 1.5°K.

According to Cade,[25] the ion is bound to a vortex ring with some potential V(r) which depends only on the distance r between the ion and the vortex core. If an electric field is present, the ion will then be bound with some energy

$$W = eV(r) - eEr. \tag{10}$$

Then the escape probability will have the form

$$P_r = P_o \exp(-W/kT) = P_o \exp(-(eV-eEr)/kT), \tag{11}$$

where k is the Boltzmann's constant.

Persistence Current

Several years ago, Bruschi, Maraviglia and Mazzoldi[28] (hereafter referred to as BMM) discovered that negative ions could pass through a field free region after they had passed through a region where the applied electric field was above E_{c2} (refers to Figure 1). They named this phenomenon the "persistence" of the drift velocity of the ion. In order to understand their discovery, they made a series of measurements on the average drift velocity of ions, second sound attenuation and the retarding potentials needed to stop the persistence currents. Their results indicated that the onset electric field for a decrease in

the amplitude of the second sound wave and the onset field of the persistence current both occured at the same field E_{c2}. Figure 8 shows BMM's result at a temperature of $0.916^{\circ}K$. Where v_d represents the average drift velocity of the ion, ΔA is the decrease in the amplitude of the second sound wave (thermal wave) due to the ion beam, and I is the persistence current. The persistence current increased linearly with the applied electric field and was able to pass through a high retarding electric field.

The two-fluid nature of superfluid liquid helium leads to a new type of wave propagation known as "second sound".[29,30] Second sound is a temperature wave, in which the normal and superfluid components move out of phase in opposite directions. Since the superfluid component is colder than the normal component, an increase in the concentration of the superfluid component at a point lowers the temperature there, while a half wavelength away, an increase in the concentration of the normal component raises the temperature.

BMM found a linear dependence of the second sound attenuation upon the electric field. Theoretically, the second sound attenuation should be proportional to the length of the vortex core, which is $2\pi R$, where R is the radius of the vortex ring. Since the equilibrium radius of a vortex ring varies exponentially with the electric field, a vortex ring model of persistence current should have an exponential dependence of the second sound attenuation upon the electric field. Thus BMM's linear dependence is in clear contradiction with the predicted exponential dependence of a vortex ring model. Because they were unable to interpret the second sound attenuation in terms of a single vortex

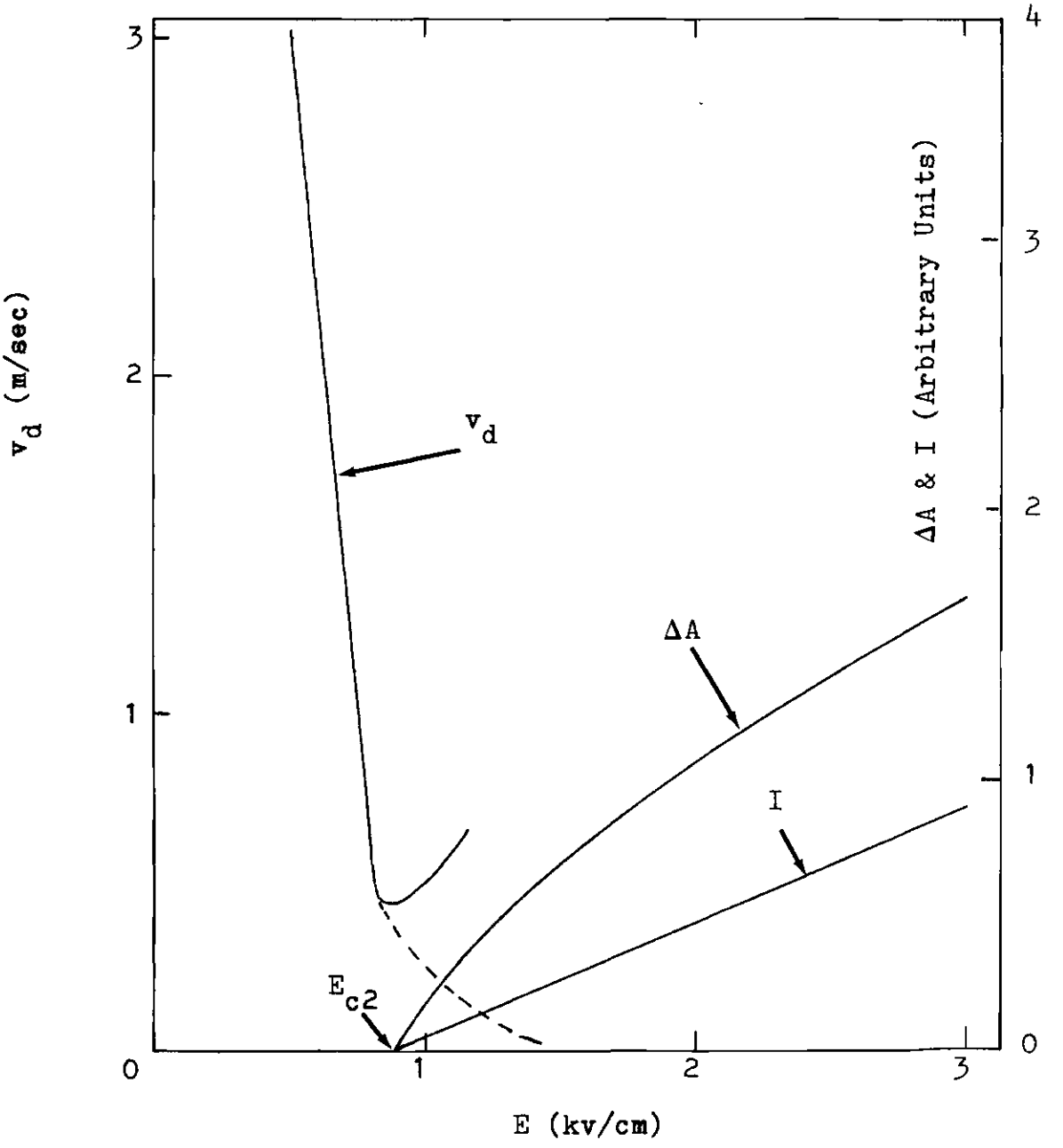

Figure 8. BMM's Experimental Results at 0.916°K

v_d: Average Drift Velocity (Dashed line indicates the result of the second paper)

ΔA: Second Sound Attenuation

I; Persistence Current

ring model, they believed the persistence current to be some kind of unknown hydrodynamic entity bound to an ion.

However, in a later paper,[10] Bruschi and Santini claimed that persistence current was an ion bound to a vortex ring at high electric fields. They used a different technique to measure the average drift velocity of the ion and found that the minimum which appeared in the first paper was not real. Instead, they found that the average drift velocity continued to decrease as the electric field increased as indicated by the dashed line in Figure 8. They claimed that the first measurement was incorrect and the minimum in the velocity curve was not real because the first technique was not accurate when used to measure the velocity of energetic particles.

The authors of the second paper did not discuss the second sound attenuation. Padmore[13] later would explain that a vortex ring in high electric fields did not have time to reach its equilibrium radius before being collected. Its maximum radius varied linearly with the electric field. This would explain the linear dependence of the second sound attenuation upon the electric field in BMM's first paper.

Padmore[13,14] has recently made a theoretical analysis of persistence currents by assuming that persistence currents are ions trapped in vortex rings. He assumed that the escape probability of ions from vortex rings was very small after the vortex rings had entered the field free region. The crucial consideration was whether these ion-ring complexes had enough energy to cross the field free region and reach the collector. Figures 9 and 10 are the theoretical

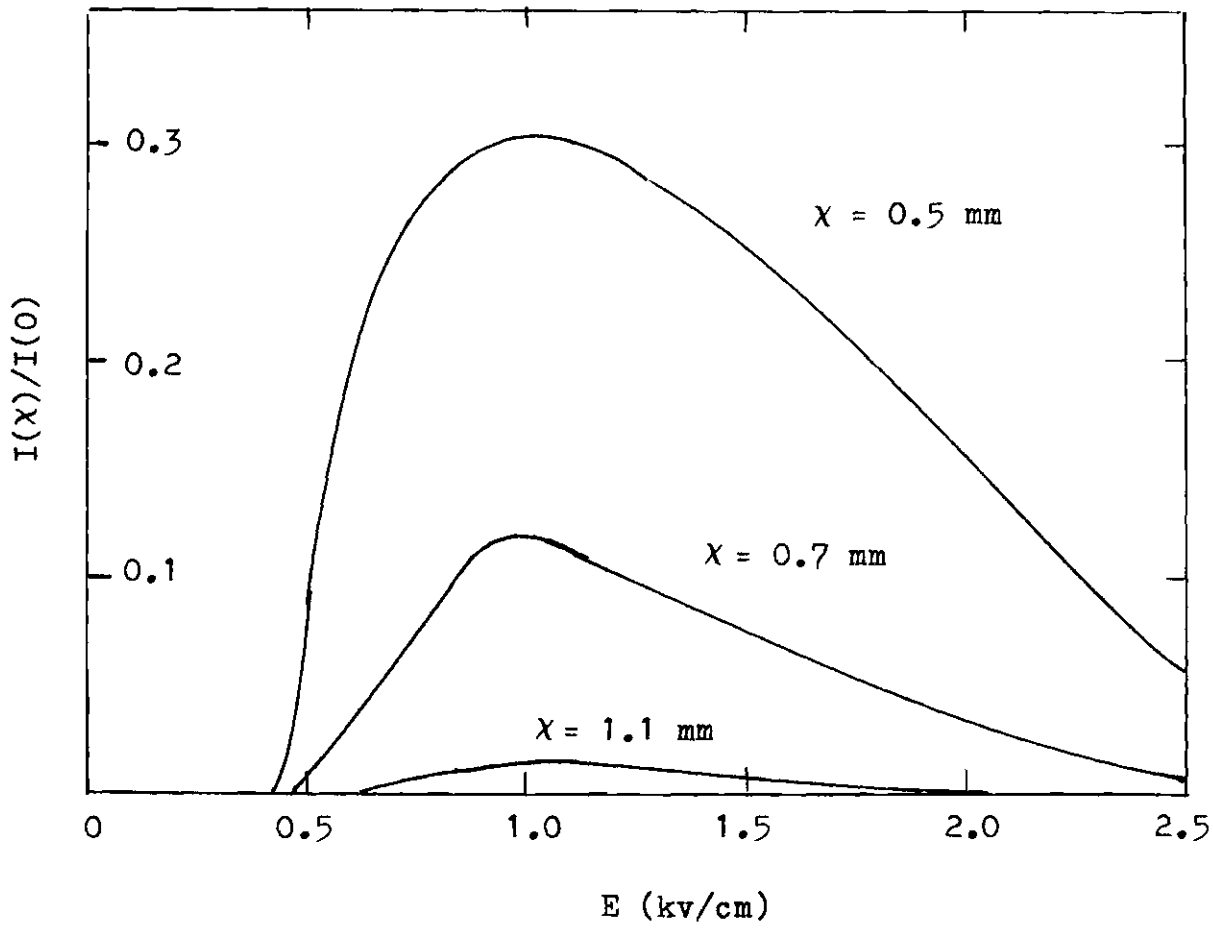

Figure 9. Persistence Characteristics of Positive Ions near 0.85°K. (After Padmore)

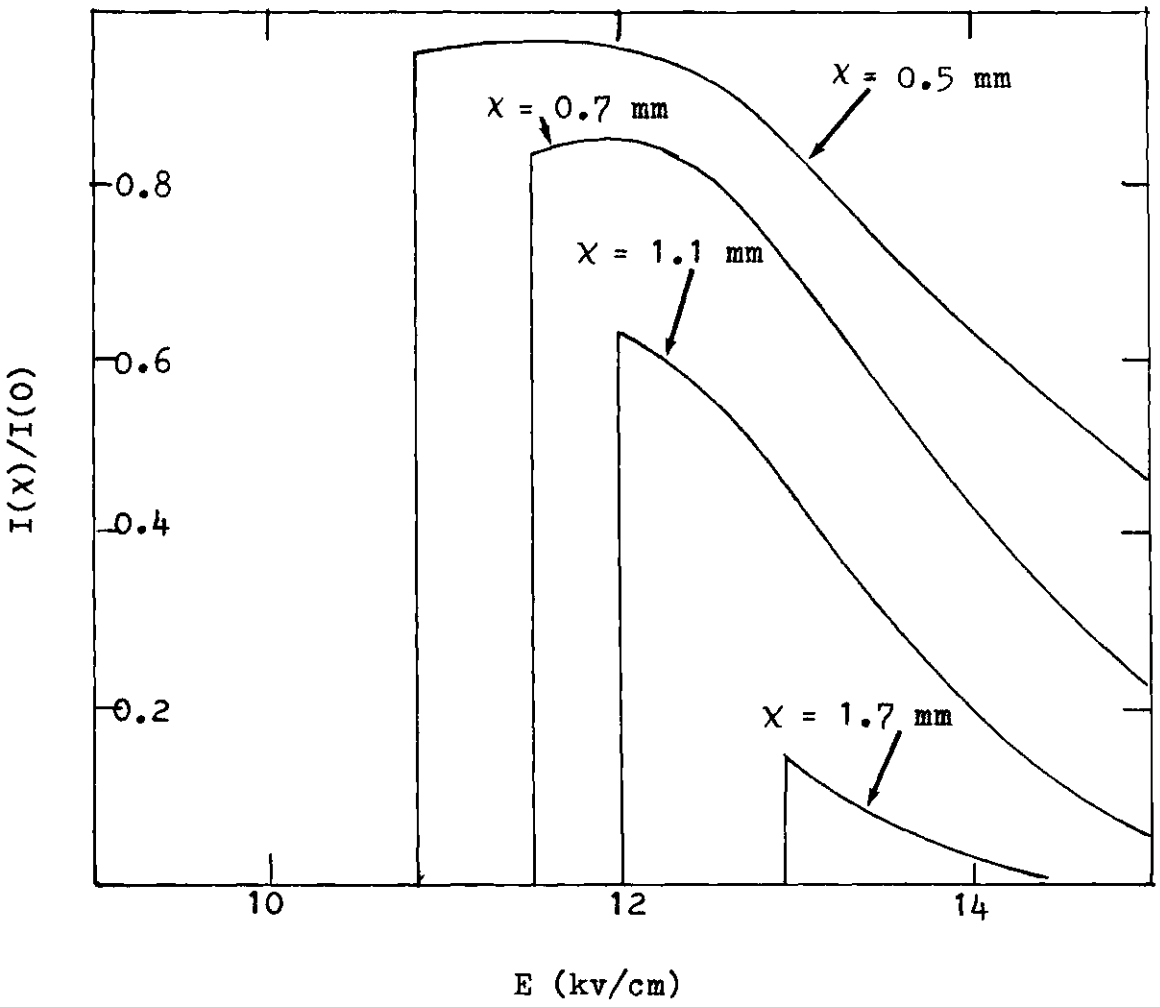

Figure 10. Persistence Characteristics of Negative Ions near 1.2°K. (After Padmore)

calculations made by Padmore. Figure 9 indicates positive persistence currents collected at three different distances X in the field free region at a temperature near 0.85°K. Figure 10 represents similar results for negative ions at a temperature near 1.2°K. The persistence current begins to be measurable when the applied electric field is large enough to give the vortex ring enough energy to cross the field free region. Longer field free distances require larger accelerating electric fields. Ion escape probabilities were needed in Padmore's calculations. For positive ions, he used the escape data measured by Cade.[25] As for negative ions, only zero-field escape data were available. It was necessary for Padmore to extrapolate the zero-field escape data measured by Dauglass[27] to obtain high field escape probabilities for negative ions. It is not certain that such extrapolations produce accurate escape data for non-zero electric fields. The escape probability affects the shape of the persistence current curve. The sharp edges at the beginnings of Padmore's negative persistence current curves are due to the small escape probabilities he used. Padmore's suggestion that persistence currents are ions trapped in vortex rings is attractive for several reasons. The combined influences of temperature and electric field will produce vortex rings large enough to be able to cross macroscopic field free distances. This would explain the existence of persistence currents. Also, large vortex rings would be able to produce second sound attenuation. It was our intention to begin this research by making a series of range or size measurements and using Padmore's theory to determine the escape probabilities for negative ions.

The farthest distance a vortex ring will travel in a field free region is defined as the "range" of the vortex ring. A relation between the range of a vortex ring and its size can be derived as follows. In equations (5), (7) and (8), we have that the velocity, energy and momentum of a vortex ring are

$$v = (\kappa/4\pi r)(\ln(8r/a) - \tfrac{1}{4}). \tag{5}$$

$$\epsilon = \tfrac{1}{2}\rho\kappa^2 r(\ln(8r/a) - 7/4). \tag{7}$$

$$p = \pi\rho\kappa r^2. \tag{8}$$

In a field free region, the total force acting on the vortex ring will be the frictional force only, which is

$$F = \frac{dp}{dt} = -\alpha(\ln(8r/a) - \tfrac{1}{4}). \tag{12}$$

From equations (8) and (12), we have

$$dp = 2\pi\rho\kappa r dr$$

and

$$dt = \frac{-dp}{\alpha(\ln(8r/a) - \frac{1}{4})}$$

$$= \frac{-2\pi\rho\kappa r dr}{\alpha(\ln(8r/a) - \frac{1}{4})}. \tag{13}$$

Substituting equations (5) and (13) into the relation $dx = vdt$, we find

$$dx = (\kappa/4\pi r)(\ln(8r/a) - \tfrac{1}{4})\,\frac{-2\pi\rho\kappa r dr}{\alpha(\ln(8r/a) - \frac{1}{4})}$$

$$= \frac{-\rho\kappa^2}{2\alpha} dr \ . \tag{14}$$

Integrating equation (14), we get a relation between the size and the range of a vortex ring

$$R_o \approx 2\alpha\rho^{-1}\kappa^{-2}x_o \ , \tag{15}$$

where R_o is the initial radius of the vortex ring which is assumed large, and x_o is the range of the vortex ring. The energy of such a ring is

$$\epsilon = \tfrac{1}{2} \rho\kappa^2 R_o(\ln(8R_o/a) - 7/4). \tag{16}$$

Therefore measurement of the size of a vortex ring directly implies knowledge of its range and its energy. The size can be measured by placing a particular size of grid in the path of the ion beam. If the vortex rings have a size smaller than the opening of the grid as they reach the grid, some of them will pass through the grid and reach the collector. If their size is larger than the grid opening as they reached the grid, they will be stopped by the grid and no current will be measured by the collector. Hence the size of a vortex ring can be measured by varying the size of the grid.

Contributions of This Research

A series of investigations have been made during the course of this thesis project to examine the high electric field behavior of negative ions in superfluid helium. The contributions of this research

to the study of superfluid helium are as follows:

1. Theoretical calculations of the persistence current onset fields using a vortex ring model have been compared with our experimental results. It is concluded that the persistence ion complex is not an electron trapped in a circular, singly quantized vortex ring.

2. The size of the ion complex has been analyzed and is found to be about 35 microns, almost independent of electric field and temperature.

3. The creation of the persistence ion complex has been studied. It has been concluded that creation can take place while the ion is in the vortex ring state.

4. The behavior of the persistence ion complex in very high electric fields has been observed. It has been discovered that the persistence ion complex breaks up at sufficiently high electric fields.

CHAPTER II

EXPERIMENTAL APPARATUS

Cryogenic Apparatus

The cryogenic apparatus consists of a four-inch inner diameter helium dewar surrounded by a nitrogen dewar.[31] The helium dewar is mounted on an apparatus flange. A Kinney Vacuum KT150 Triplex Pump with a 152 ft^3/min free air displacement is connected to the flange. Pumping speed is controlled by a diaphragm valve.[32] The vapor pressure of the liquid helium which indicates the temperature of the cryostat is measured by a manometer. The manometer is connected to the cryostat by a quarter-inch inner diameter stainless steel tubing extended below the helium level. A 0.1-inch diameter constriction is made near the bottom of the tubing to avoid a helium gas resonance. At the early stage of this experiment a short tubing which was exposed to the helium vapor far above the liquid helium surface was used. No significant difference was observed between these measurements and those with a long tubing.

Various electrical leads were brought out of the cryostat through a specially designed feed-through, as shown in Figure 11. This feed-through was made through the following procedures: A brass hollow tube was filled with Stycast 2850 GT Epoxy,[33] through which bare wires were introduced. Electrical leads were protected with teflon tubing at the two epoxy surfaces to prevent possible electrical discharge

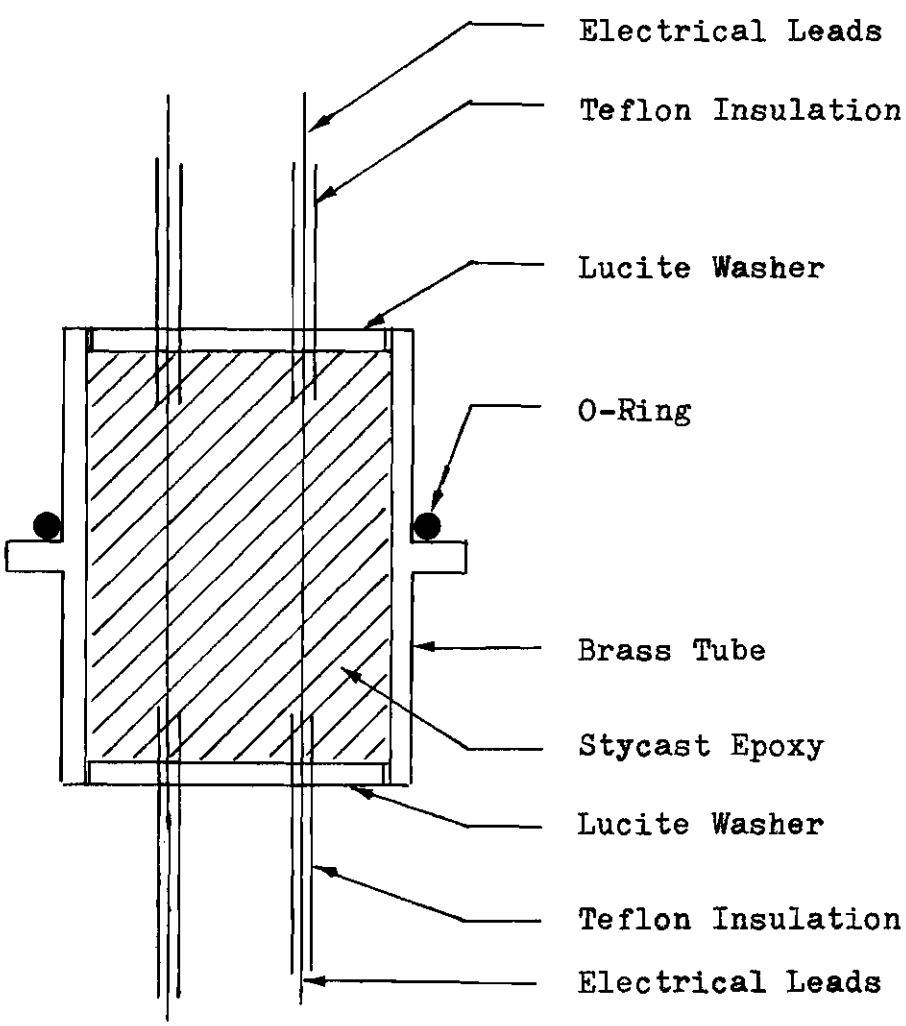

Figure 11. Vacuum Tight Electrical Feed-Through

through air or hilium vapor. Two lucite washers were placed at both ends of the brass tube to prevent the epoxy from flowing out and also to hold the wires straight. The advantages of this feed-through are the vacuum-tightness[34] and the good insulating properties of the Stycast Epoxy. Voltages of up to 8,000 volts have been successfully applied to it without a breakdown. All the high voltage leads inside the helium dewar were insulated with teflon tubing.

Sample Holder

The sample holder was made of brass and insulated with teflon. Three 0.375-inch diameter brass posts covered with 0.125-inch thick teflon hollow cylinders were bolted on a 2.5-inch diameter brass plate. These three posts were equally separated and a 1.20-inch diameter circular clearance was left at the center of the brass plate. Figure 12 shows the detailed experimental arrangement which consists of a source and a collector separated by grids and spacers. The radioactive source (Americium-241, 19μ Ci) was mounted at the center of an 1.20-inch diameter circular nickel plate. The collector was connected to a vibrating reed electrometer[35] by a coaxial cable consisting of thin wall stainless steel tubing and a stainless steel wire insulated with teflon tubing. Nickel grids[36] were spot welded between two phosphor bronze plates which were 0.010-inch thick and 1.20-inch in diameter. The diameter of the exposed grid was 0.125 inch. The grid and plates were then gold plated with Atomex Immersion Gold Solution.[37] Circular teflon spacers of various thickness were placed between each pair of source, grids and collector to keep them parallel and insulated from

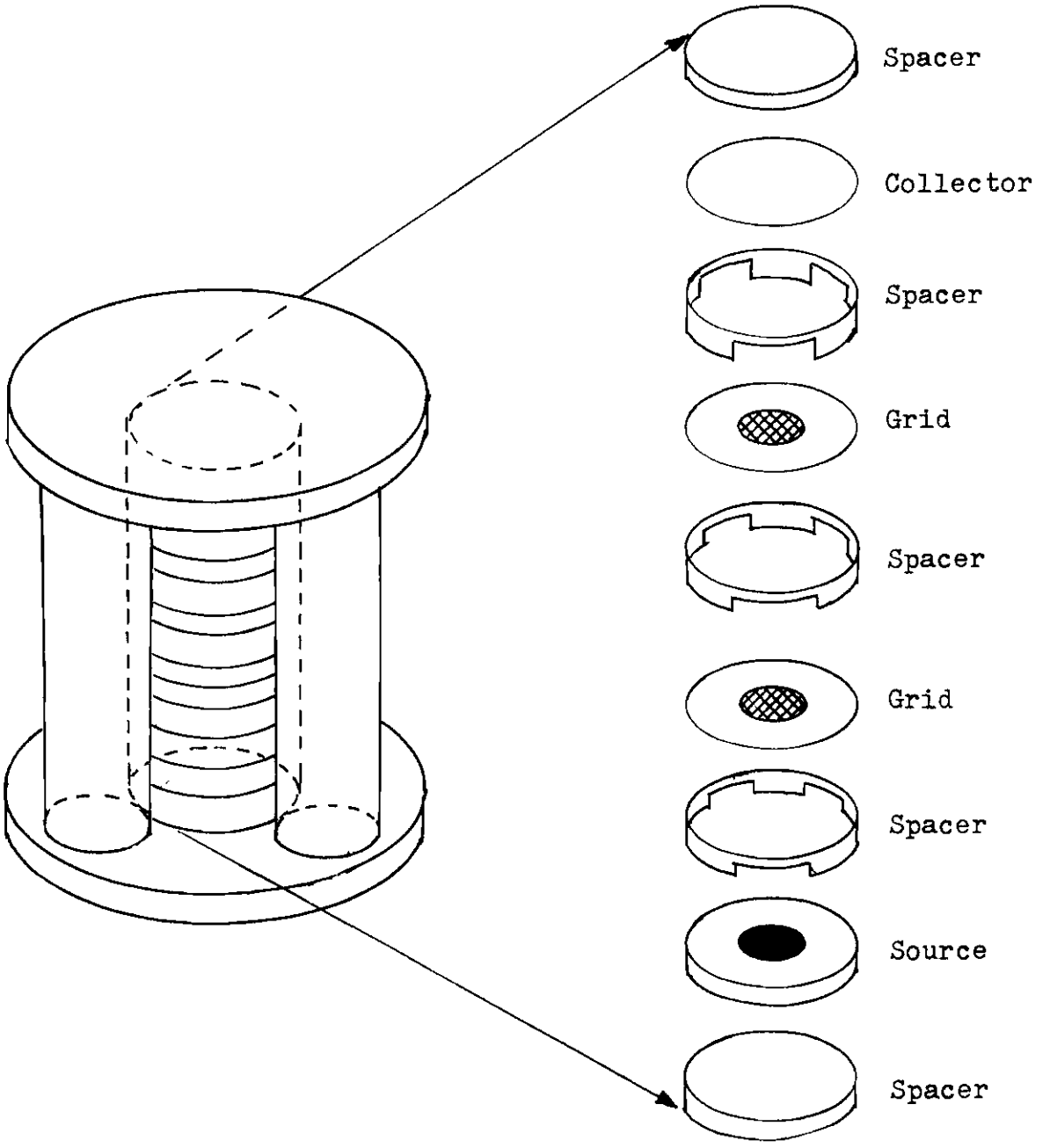

Figure 12. Sample Holder

each other. Three grooves were made on each spacer to provide room for electrical leads and admit liquid helium to the grid space. Because all the grids, spacers, collector and source were made of the same diameter and the three rigid posts of the sample holder made a uniform circular clearance at the center, it was very easy to line up the source and the grids at the center. Samples touched the posts only at three points and the teflon surfaces of the posts had low friction, hence samples could be changed easily from time to time.

Electrical System

Figure 13 is a diagram of the electric system for the ion measurements in this research. A 400-volt battery system is applied to a five-millimeter space between the source and the first grid. This constant electric field is used to initiate the ion current. An accelerating power supply[38] which can be regulated up to 8,000 volts is used across a 6-mm space between the first and the second grid. Vortex rings and persistence currents are created in this high electric field region. A current control power supply[39] which has available high voltage up to 4,000 volts is connected between the second grid and the collector. (Actually it is connected between the grid and ground, the input of the electrometer is held near grounded, the potential drop across the electrometer is less than 10^{-4} volt.[40].) The electrometer can measure current between 10^{-17} ampere and 10^{-7} ampere.

Temperature Measurements

Since temperature plays an important role in superfluid helium experiments, it is essential to choose an accurate and sensitive method

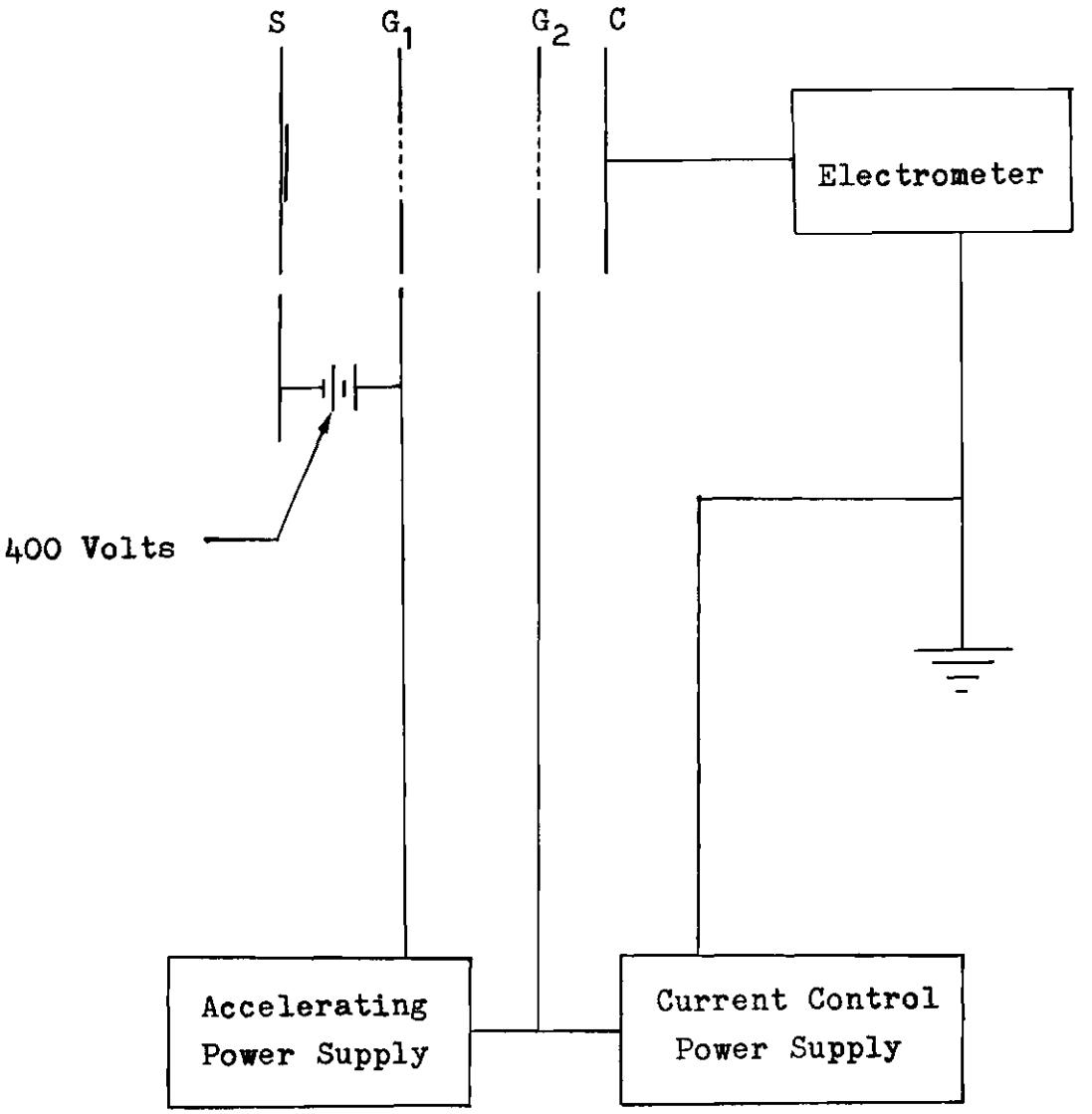

Figure 13. Electrical System for Ion Measurement

to measure the temperature. The thermometer we used in this experiment is a helium vapor pressure thermometer. The vapor pressure of a substance decreases as the temperature falls and so this pressure may be used as a measure of temperature. Vapor pressure thermometers do not usually need calibration because the vapor pressures of condensed gases used in low temperature work have been accurately measured and the values tabulated as function of temperature. A He^4 vapor pressure thermometer is among the most frequently used methods in low temperature experiments. Figure 14 shows the arrangement which we used in this experiment. The long stainless steel tube, which extends below the liquid helium level, is designed to reduce the error arising from any drop in pressure that may result from the flow of gas when the liquid is being pumped. The constricted part near the end of the long tube was made to avoid a helium gas reaonance. The range over which a vapor pressure thermometer may be used extends from the noraml boiling point of the liquid to the temperature at which the vapor pressure becomes immeasurably small. A U-shape mercury manometer may be read by eye to an accuracy of about ± 0.2 mm, which means that temperatures can be measured down to $1.7^{\circ}K$ with an accuracy of one percent. For lower temperatures, a simple U-shape tube filled with a light oil may be used to determine lower vapor pressures. Butyl phthalate is a suitable fluid for this application. Its vapor pressure at room temperature is less than 10^{-3} mm of Hg and its density (1.04 gm/cm^3) is about 13 times less than that of mercury, so that pressures 13 times lower can be measured to the same percentage accuracy.[41,42] At temperature around $1.2^{\circ}K$, the accuracy is about one-hundredth of

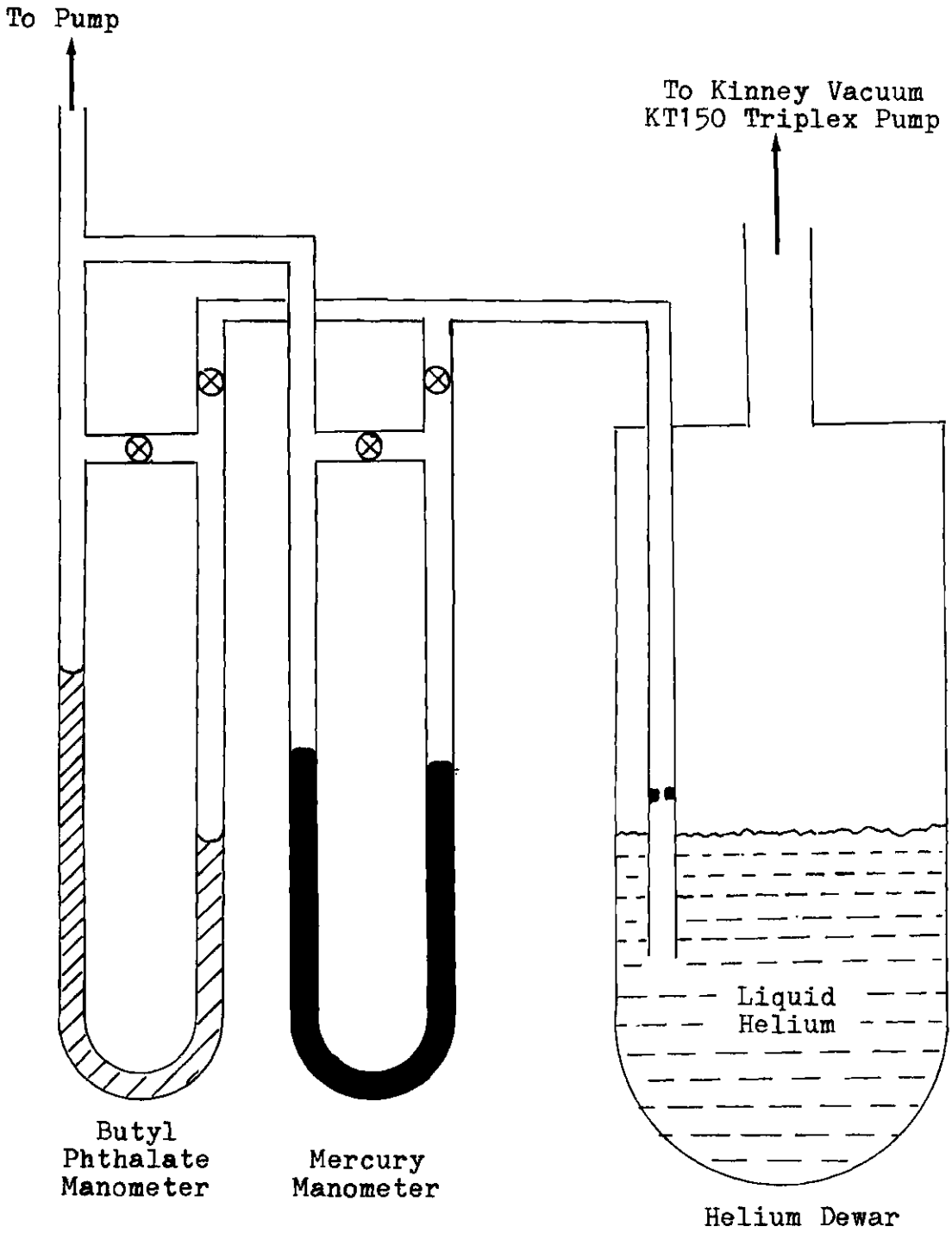

Figure 14. He^4 Vapor Pressure Thermometer

a degree. Vapor pressures are converted into temperatures with a standard table.[43]

CHAPTER III

EXPERIMENTAL RESULTS

Four factors can be varied in the measurements of this experiment, the temperature, the applied electric field, the grid size, and the distances between each pair of source, grids and collector. Temperature can be controlled by the valve, and the electric field can be varied easily outside the cryostat. However, the other two factors can only be changed inside the helium dewar. Nothing can be changed inside the cryostat after it has been cooled down. Therefore only one grid size and certain distances between samples are involved in the measurements of each run.

Vortex Ring and Persistence Current

Persistence current has been claimed to be an ion trapped in a vortex ring by both experimental[10] and theoretical[13,14] physicists. The dynamical and frictional properties of vortex rings are well established. Given the temperature T, the accelerating electric field E, and the accelerating distance S, the range of the resulting vortex ring can be calculated as follows. The dynamic behavior of a vortex ring can be represented by

$$\frac{dp}{dt} = F \tag{17}$$

In equations (5), (8), (9) and (15), the velocity, momentum, applied

forces and range of a vortex ring are

$$v = (\kappa/4\pi r)(\ln(8r/a) - \tfrac{1}{4}) = (\kappa/4\pi r)\ln(r/\xi) \tag{5}$$

$$p = \pi\rho\kappa r^2 \tag{8}$$

$$F = eE - \alpha(\ln(8r/a) - \tfrac{1}{4}) = eE - \alpha\ln(r/\xi) \tag{9}$$

$$R_o \approx 2\alpha\rho^{-1}\kappa^{-2}x_o \tag{15}$$

Substituting equations (8) and (9) into equation (17), we obtain

$$2\pi\rho\kappa r \frac{dr}{dt} = eE - \alpha\ln(r/\xi)$$

then

$$dt = \frac{2\pi\rho\kappa r dr}{eE - \alpha\ln(r/\xi)} \tag{18}$$

Using the relation $dS = vdt$ with the velocity given by equation (5), we get

$$dS = \frac{\frac{1}{2}\rho\kappa^2\ln(r/\xi)dr}{eE - \alpha\ln(r/\xi)} \tag{19}$$

Padmore integrated equation (19) and obtained

$$S(r) = \tfrac{1}{2}\kappa^2\rho\alpha^{-1}(\xi(eE/\alpha)e^{eE/\alpha}(E_1(F/\alpha)-E_1(eE/\alpha))-r+\xi) \tag{20}$$

Where E_1 is the exponential integral

$$E_1(x) = \int_1^\infty \exp(-xy)\frac{dy}{y}$$

and the initial condition is $r = \xi$ at $t = 0$. After having been accelerated in an electric field E through a distance S, a vortex ring enters a field free region with a radius R_o, which is related to E and

S by

$$S(R_o) = \tfrac{1}{2}\kappa^2\rho\alpha^{-1}(\xi(eE/\alpha)(E_1(F/\alpha)-E_1(eE/\alpha))\exp(eE/\alpha)-R_o+\xi) \qquad (21)$$

Rearranging equation (21), the radius R_o can be expressed in terms of the accelerating electric field E and the accelerating distance S. Since the range of a vortex ring and its radius are related by equation (15), its range can be calculated when the temperature, the accelerating electric field, and the accelerating distance are known.

BMM never quoted the temperature, the electric field and the field free distance together, so their results can not be used to test the vortex ring model of persistence current. We started our experiment by testing persistence currents for the presence of vortex rings. Our regular measurements used a 6-mm accelerating distance and a 3-mm field free (small retarding potential) region. When we began to suspect that persistence current might not be due to vortex rings, the field free region was increased to 6-mm (at one temperature, 1.13°K, a distance of 12-mm was used) in order to make a definitive test for vortex rings. The onset potentials of persistence current at various temperatures were determined. Figure 15 shows an example of our data obtained with a 232-μ grid at a temperature of 1.13°K. The onset electric potential for persistence current is 2,600 volts at this temperature. With the onset electric potential known, we are in a position to compare this experimental result with the onset potential of a vortex ring current which can be calculated from the known dynamical properties of vortex rings.

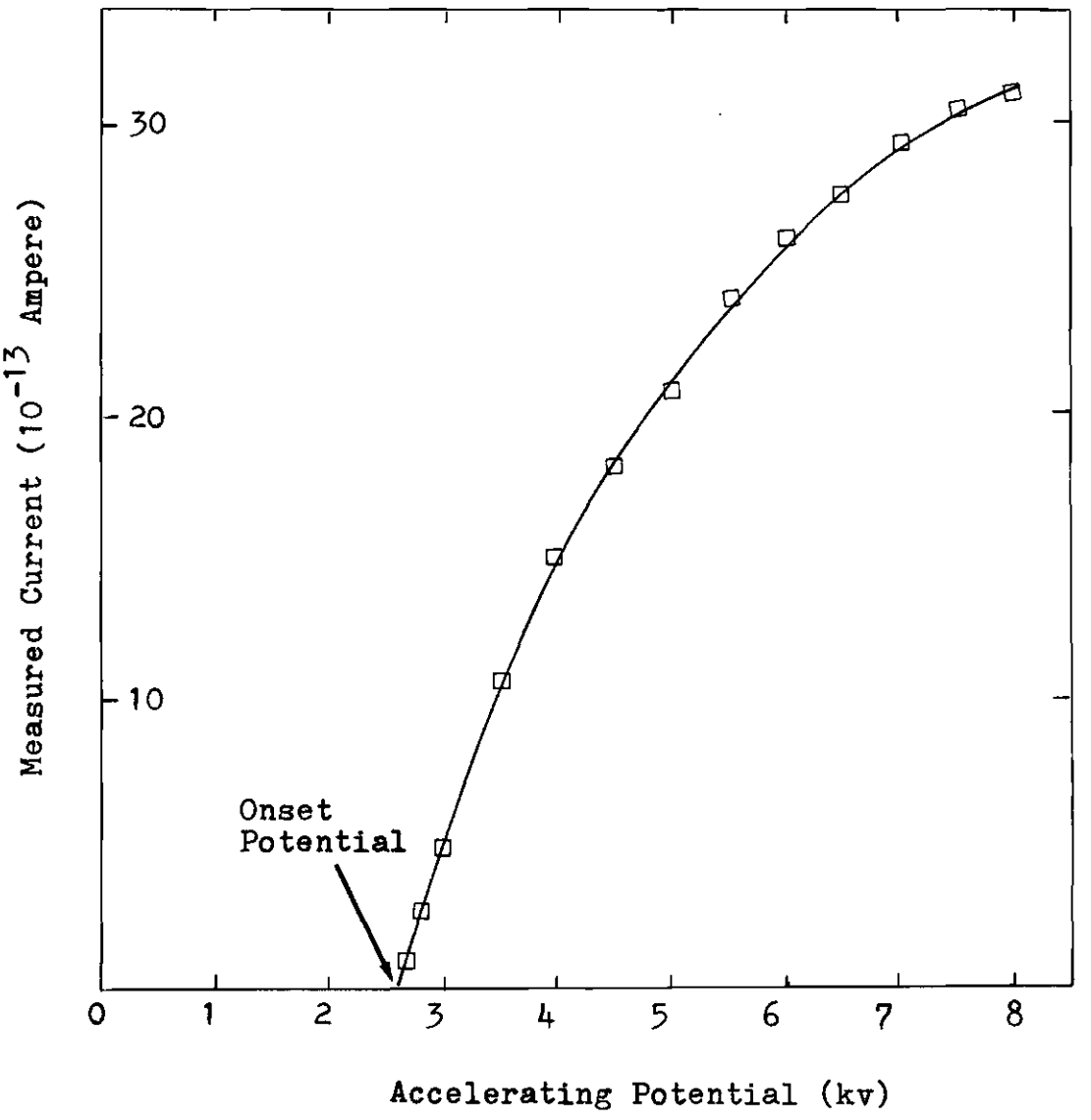

Figure 15. Persistence Current of 232-μ Grid at 1.13°K

Range

Our experimental measurements indicated that persistence currents were able to cross a 12-mm field free region at a temperature of 1.13°K, hence our measured persistence current has a range with a lower limit of 12-mm as shown by the horizontal line in Figure 16. The curved line in Figure 16 represents the range of a vortex ring and the vertical dashed line indicates the onset potential of our measured persistence current at this temperature. At the onset potential our measured persistence current has a range of at least 12-mm, while a vortex ring has a range of 0.01-mm, a difference of three orders of magnitude. At point P, the vortex ring has a range equal to 12-mm, but it would require an onset potential of 14,400 volts for the vortex ring to have this range according to our calculations.

Energy

It has been pointed out in Chapter I that the size, range, and energy of vortex rings are related to each other. Let us now compare our measured persistence currents with vortex rings from an energy point of view. Figure 17 indicates the relations between the significant energies and the applied electric potential at 1.13°K. The curved line represents the calculated energy of a vortex ring at each applied electric potential, the horizontal straight line is the energy necessary for a vortex ring to corss a 12-mm field free region, the inclined straight line indicates the maximum energy available to a vortex ring from the electric field, and the vertical dashed line is the onset potential of our measured persistence current. At the onset potential, the energy available to a vortex ring from the electric field is only

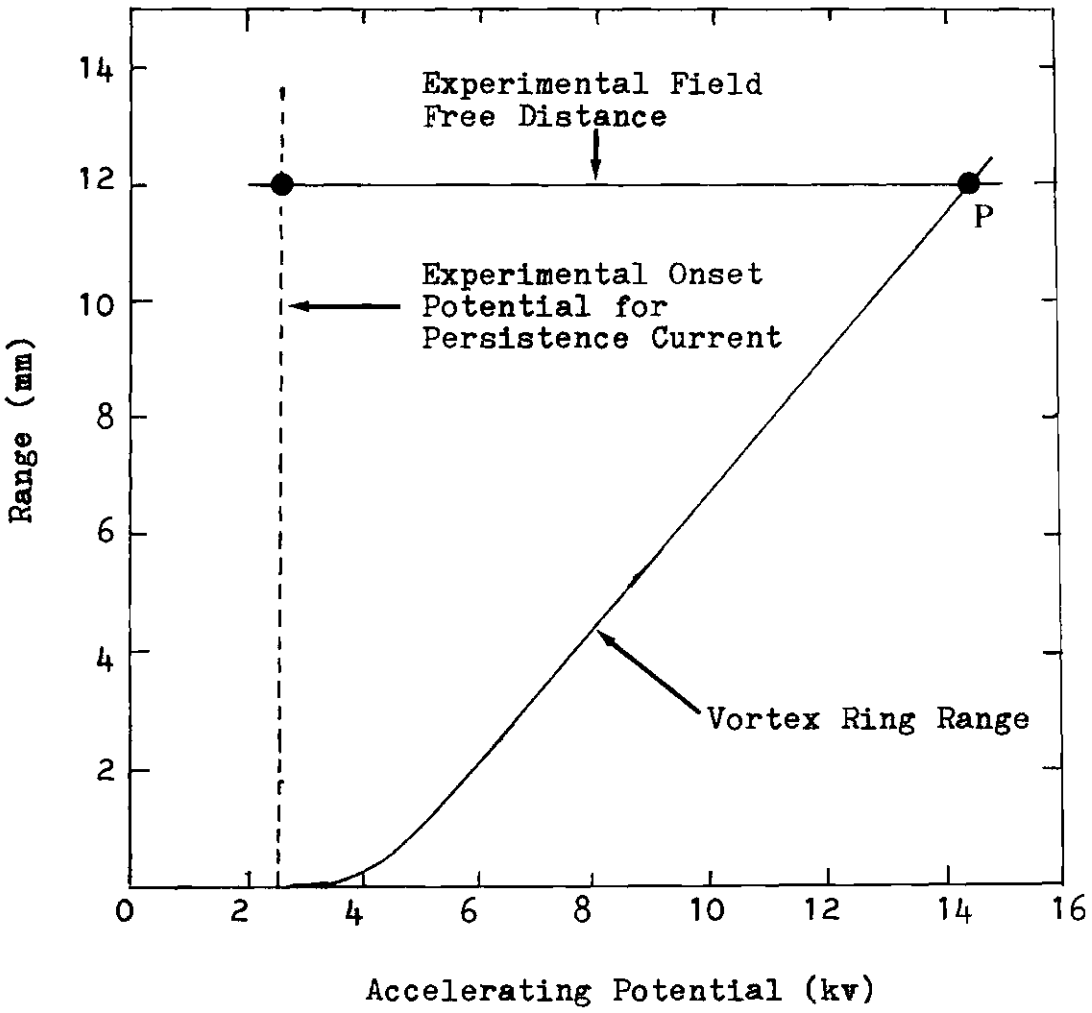

Figure 16. Range Comparison between Persistence Ion Complex and Vortex Ring at 1.13°K

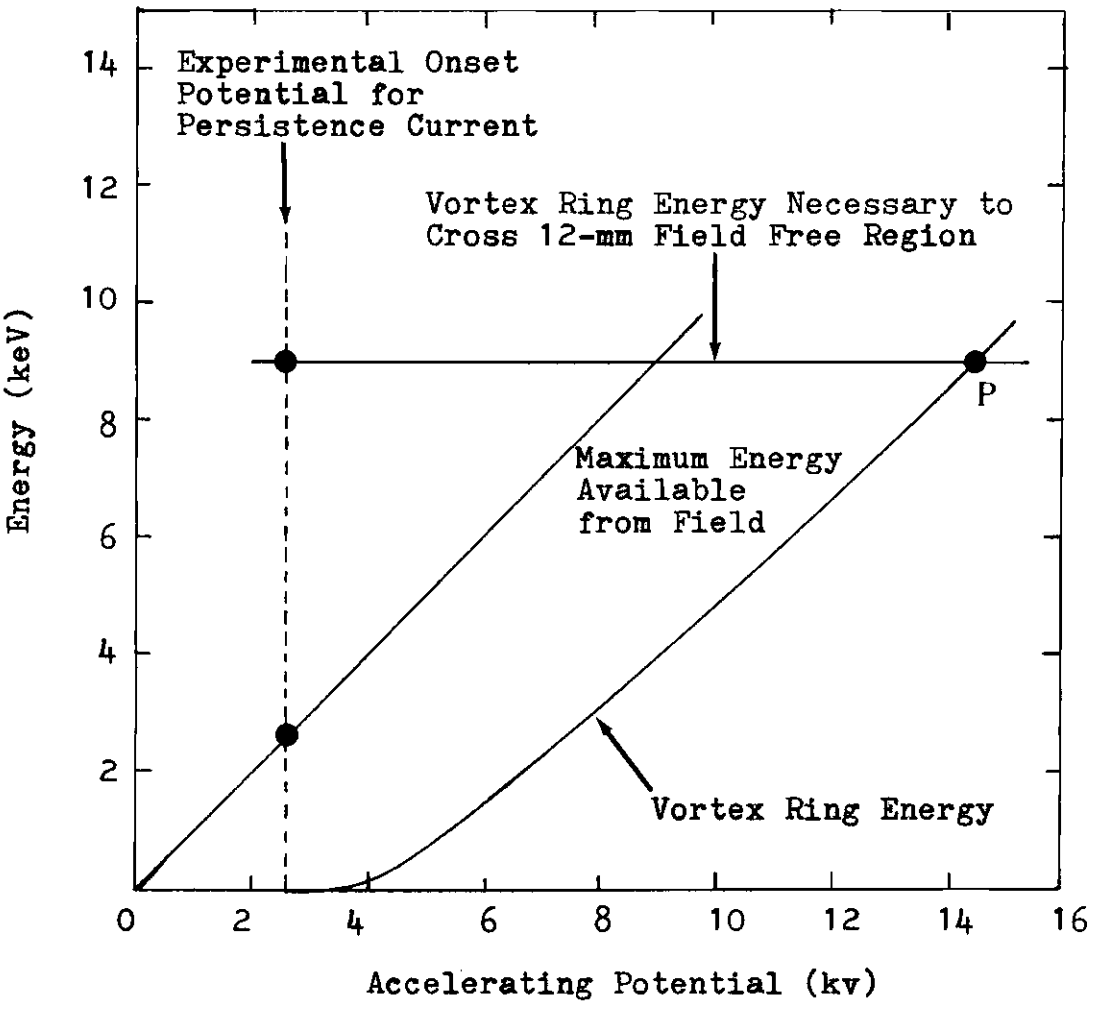

Figure 17. Energy Comparison between Persistence Ion Complex and Vortex Ring at 1.13°K

2.6 keV, but the energy required for a vortex ring to cross a 12-mm field free region is 9.0 keV which is more than three times larger. Furthermore, the energy of a vortex ring at this onset potential is only 0.001 keV, four orders of magnitude less than the energy necessary for the vortex ring to cross the 12-mm space. At point P, a vortex ring has an energy equal to the energy necessary for a vortex ring to cross a 12-mm field free region at this temperature. As pointed out earlier, an onset potential of 14,400 volts is needed to supply such a large energy to the vortex ring.

Radius

Our last effort is to compare our measured persistence currents with vortex rings from a size point of view. In Figure 18, the radius of a vortex ring is plotted against the applied electric potential. The results for our measured persistence current are also indicated in the graph. The curved line indicates the radius of a vortex ring at each applied electric potential, the horizontal straight line is the radius necessary for a vortex ring to cross a 12-mm field free region, and the vertical dashed line indicates the onset potential of our measured persistence current. At the onset potential, a vortex ring would need a minimum radius of 135 microns to cross a 12-mm field free region. The radius of our measured persistence current, indicated by small crosses in the graph, is only about 18 microns which was small enough to pass through a 62-micron grid in our measurements. (Size measurement of our persistence current will be discussed in the next section.) The actual radius of vortex ring at this onset potential is only 0.03 micron, a difference of three orders of magnitude

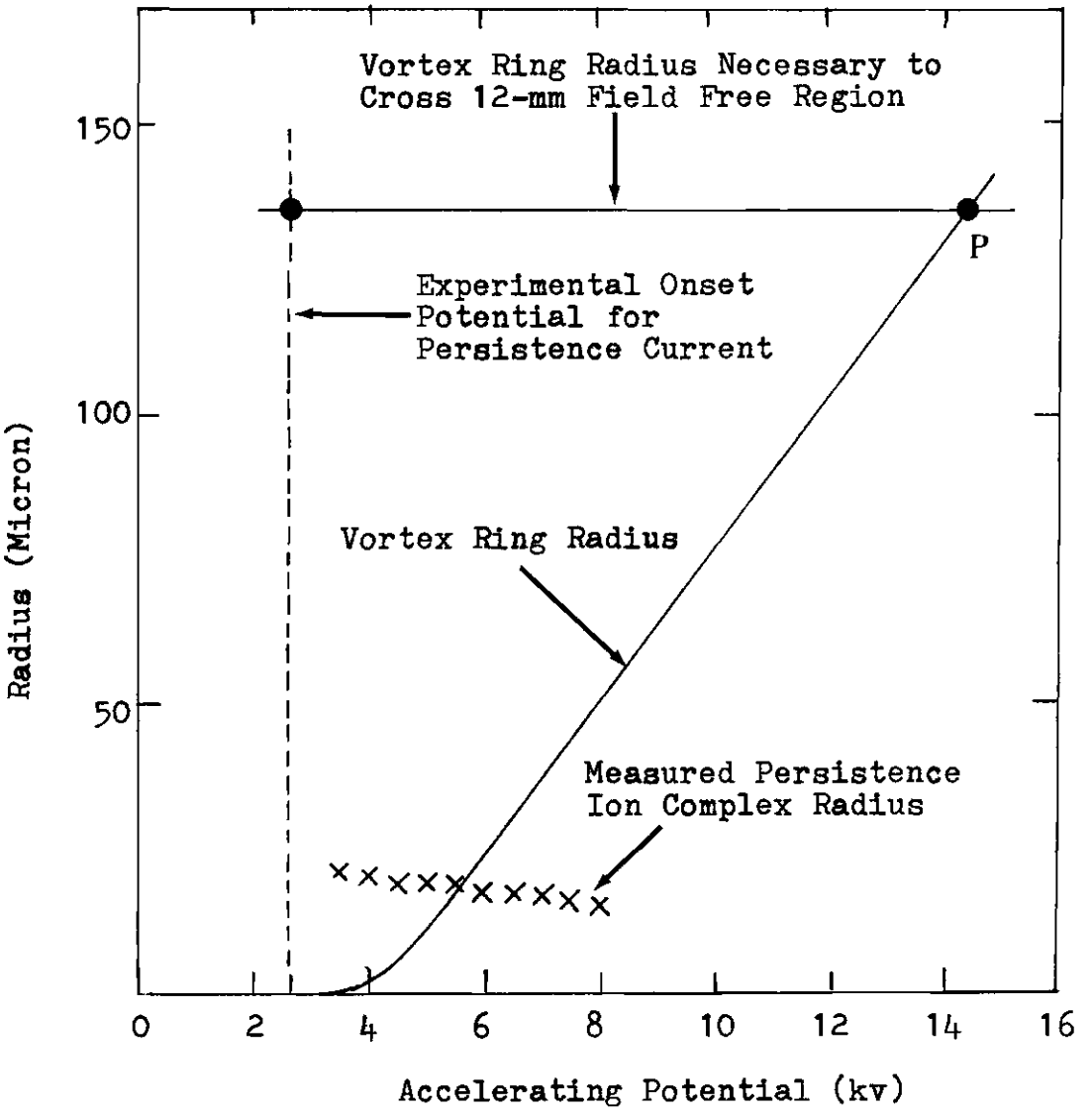

Figure 18. Radii of Vortex Ring and Persistence Ion Complex at 1.13°K

from the radius of our measured persistence current. At point P, the radius of a vortex ring is equal to the vortex ring radius necessary to corss a 12-mm field free region. This vortex ring radius is more than seven times larger than the radius of our measured persistence current.

Similar comparisons in range, energy and radius between vortex rings and our measured persistence ion complexes with a 6-mm field free region at temperatures of 1.17°K, 1.21°K and 1.24°K are listed in Table 1.

In Figure 19, the calculated onset potential of vortex rings and the observed onset potential of persistence current are plotted against temperature. It is obvious that vortex rings need potentials much larger than the persistence onset potential to cross a 6-mm or a 12-mm field free region. No ion escapes were considered in the calculation of vortex ring onset potentials. This means that these are the maximum values of range, energy and radius of a vortex ring under each circumstance. Escapes will reduce these values and even larger onset potentials will be required for vortex rings to cross the field free region.

All of the above discussion indicates that it is very unlikely that persistence current is due to vortex rings.

Most of our measurements were made with small retarding potentials. However, we did verify BMM's result that persistence currents can pass through large retarding potentials. A retarding potential up to 4,000 volts was applied and persistence currents were still observed. If persistence current is due to vortex rings, this implies the presence

Table 1. Comparisons Between Vortex Ring and Persistence Ion Complex

	Temperature		
	1.17°K	1.21°K	1.24°K
Experimental Onset Potential V_o for Persistence Ion Complex (Kilovolt)	3.65	4.80	5.90
Range of Vortex Ring at V_o (Millimeter)	0.0041	0.0045	0.0050
Range of Persistence Ion Complex at V_o (Millimeter)	≥6.0	≥6.0	≥6.0
Onset Potential Required for Vortex Ring to Cross 6-mm Field Free Region (Kilovolt)	12.3	16.0	19.2
Energy Required for Vortex Ring to Cross 6-mm Field Free Region (KeV)	5.6	7.2	8.9
Energy Available at V_o (KeV)	3.6	4.8	5.6
Vortex Ring Energy at V_o (KeV)	0.02	0.03	0.04
Radius Required for Vortex Ring to Cross 6-mm Field Free Region (Micron)	88	113	135
Radius of Vortex Ring at V_o (Micron)	0.06	0.09	0.12
Measured Persistence Ion Complex Radius at V_o (Micron)	17.5	18.0	---

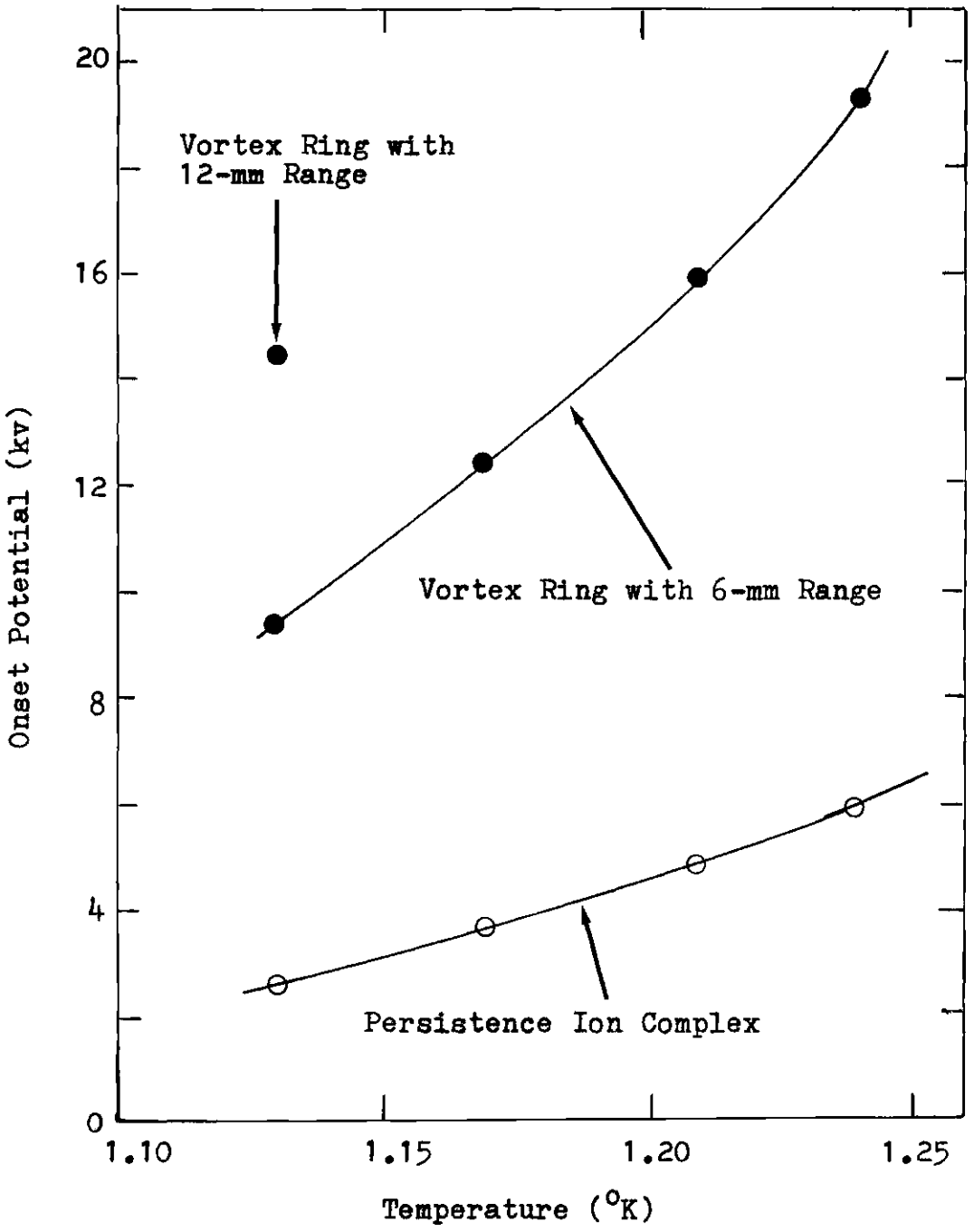

Figure 19. Onset Potentials for Vortex Rings and Persistence Currents at Various Temperatures

of vortex rings with energies of 4,000 eV. The diameter of a vortex ring with an energy of 4,000 eV is 130 microns. We have observed that persistence currents are able to pass through grids with 62-μ openings.

Size Measurements

Gamota and Sanders[45,46] measured the size of vortex rings by varying the size of grids. Similar techniques were used in this laboratory to measure the size of the persistence ion complex. Two grids were placed between a source and a collector. The first grid opening was kept constant at 293 microns, which is large enough so even a large vortex ring can pass through easily. The second grid opening was varied through 22.5, 62.5, 109 and 232 microns. The potential between the radioactive source and the first grid was kept at a constant value of 400 volts. The potential between the first and the second grids could be varied from 500 volts to 8,000 volts which was the limit of our power supply. This was the region where the persistence ion complex was created and accelerated. For size measurements, a 5-volt retarding potential was applied across the second grid and the collector. After a persistence ion complex has been created, it will gain energy while it travels through the accelerating region between the first and the second grids. If the persistence ion complex has a size larger than the second grid opening as it reaches the second grid, it will break up and the bare ion will be collected by the grid since the bare ion is unable to overcome the retarding field. No current will be collected by the collector. On the other hand, if the size of the persistence ion complex is smaller than the grid opening

as it reaches the second grid, those which hit the grid wire will break up and be collected by the grid, but some of them will pass through the grid and reach the collector. The amount of current reaching the collector depends on the size of the persistence ion complex and the transmission of the grid. Figure 20 represents the results of the size measurements at 1.17°K. No current was collected for the 22.5-μ grid, and a small amount of current was collected for the 62.5-μ grid. These results indicate that the size of the persistence ion complex lies somewhere between 22.5 and 62.5 microns.

More detailed analysis is necessary to determine the precise size of the persistence ion complex. Assuming that the interaction between the persistence ion complex and the grid is purely geometric, we let the size of the grid opening be L and the diameter of the persistence ion complex be D, as shown in Figure 21. Then each open area on the grid will be L^2, but the area available to the ion complex for which the ion does not hit a grid wire is only $(L-D)^2$. The amount of current passing through the grid will be proportional to the ratio $(L-D)^2/L^2$, to the transmission of the grid T, and to the incident current I_o. That is

$$I = I_o T((L-D)/L)^2 \qquad (22)$$

The incident current I_o can be cancelled out in the analysis by taking the ratio of two currents. The transmission of a grid is the ratio of the opened area to the total area of the grid, that is, $T = L^2/S^2$. L and S were measured by using photomicrographs. The measured sizes and transmissions of several kinds of grids are listed in Table 2.

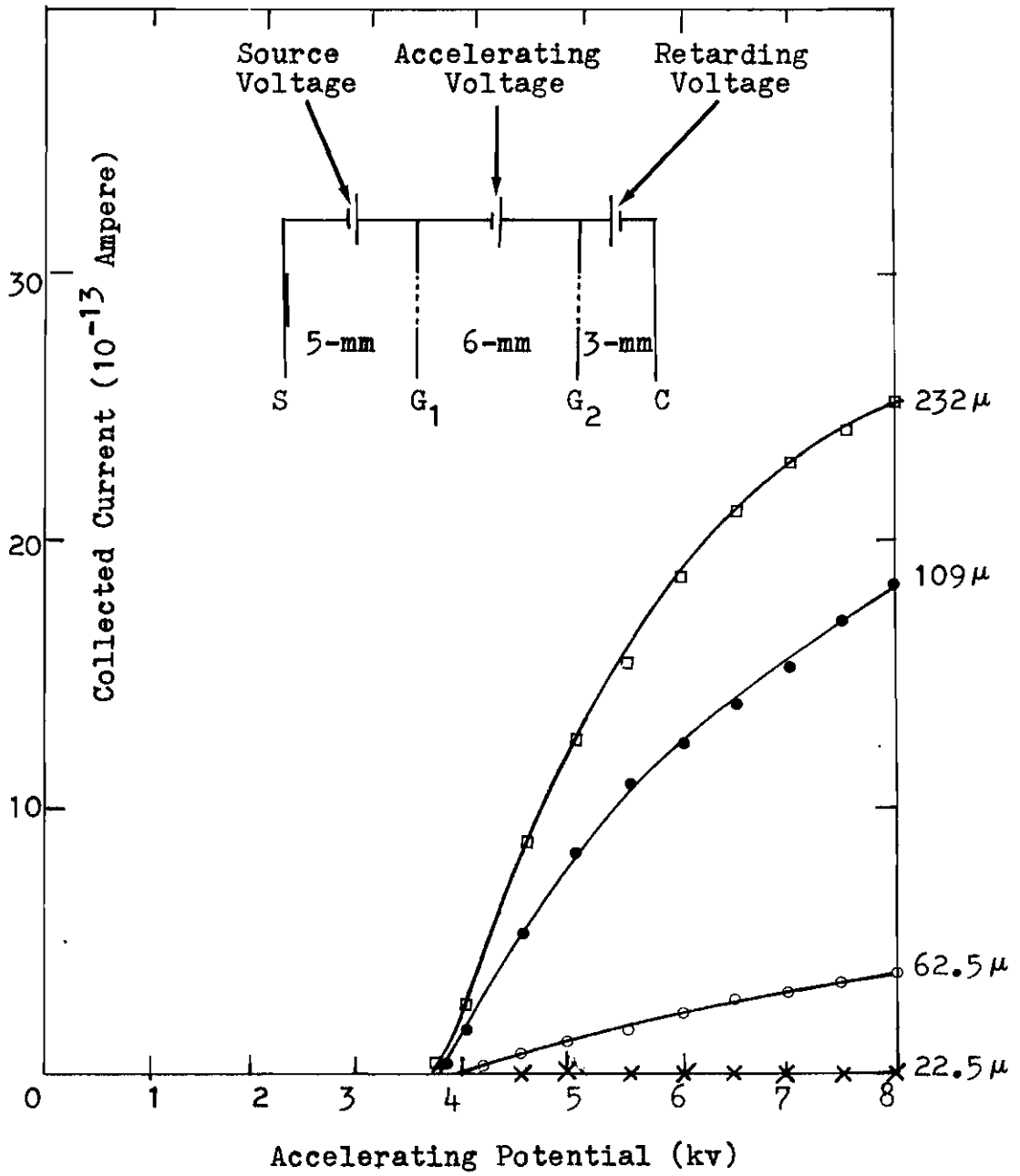

Figure 20. Collected Current vs Accelerating Potential at 1.17°K for Different Nominal Grid Sizes

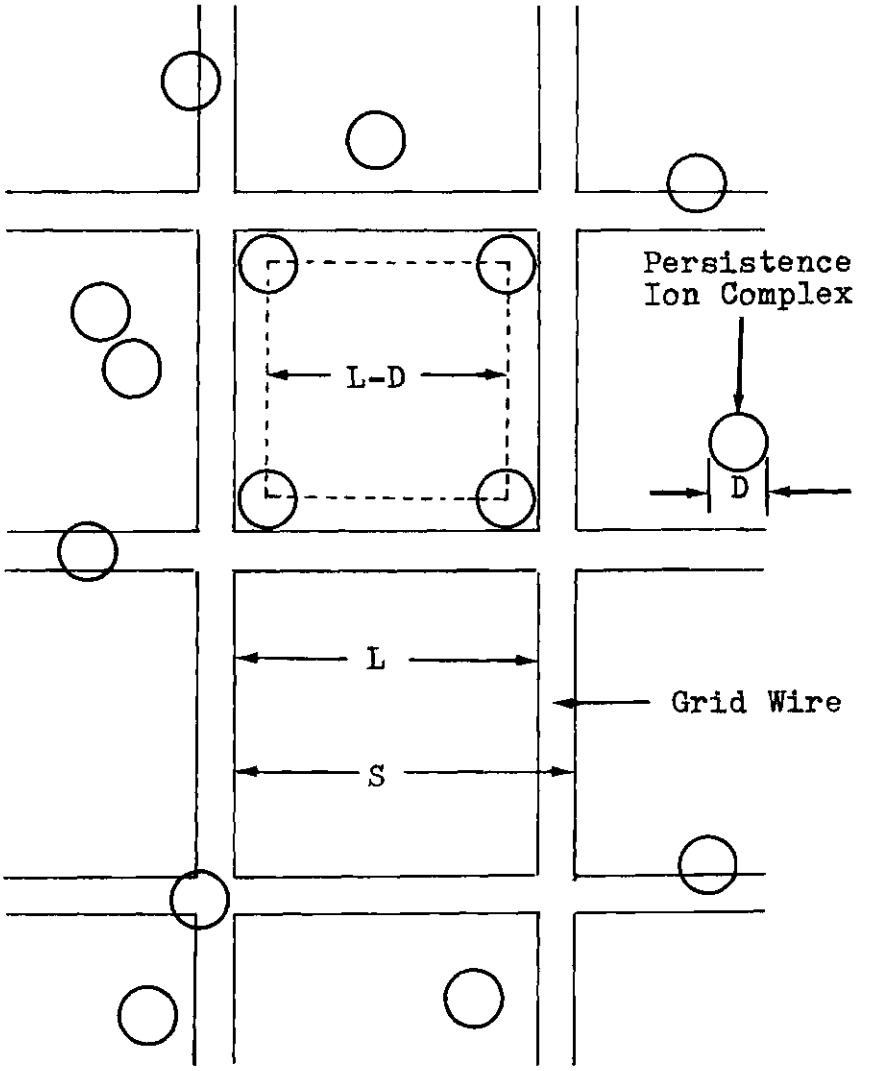

Figure 21. Grid Geometry

Table 2. Transmissions of Grids

Nominal Grid Size (Microns)	Measured Grid Size, S (Microns)	Measured Grid Opening, L (Microns)	Measured Transmission L^2/S^2
293	325	290	0.800
232	259	231	0.805
109	126	110	0.764
62.5	77.0	61.5	0.642
22.5	33.6	22.2	0.437

The application of equation (22) will be discussed as follows:

1. Size of the Persistence Ion Complex. At each accelerating potential, a best fitting value of the ion complex diameter can be determined by varying the value of the persistence ion complex diameter until minimum deviations between calculated and measured currents are obtained. Starting with equation (22), the ratio of the currents passing through two different kinds of grids at the same temperature and accelerating potential is

$$\frac{I_2}{I_1} = \frac{T_2((L_2-D)/L_2)^2}{T_1((L_1-D)/L_1)^2} \tag{23}$$

If I_1 is known, then I_2 can be calculated for a particular choice of D by

$$I_2 = \frac{T_2((L_2-D)/L_2)^2}{T_1((L_1-D)/L_1)^2} I_1 \tag{24}$$

An example of the detailed procedures in finding the best fitting value of the persistence ion complex diameter is illustrated in Appendix I. The best fitting values of the persistence ion complex diameter are plotted against the accelerating electric potential in Figure 22. The results indicate that the effective size of the persistence ion complex is slightly decreasing with the accelerating potential and almost independent of the temperature.

2. Fitting Experimental Results. The best fitting curves for three different sizes of grids at 1.13°K are shown in Figure 23. The

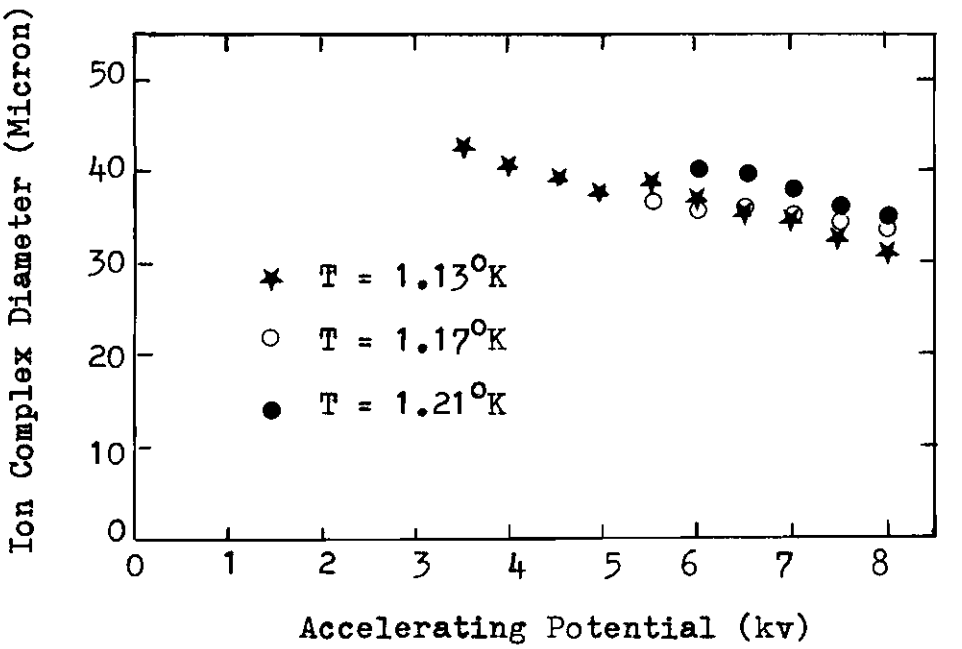

Figure 22. Best Fitting Values of Persistence Ion Complex Diameter at Three Different Temperatures

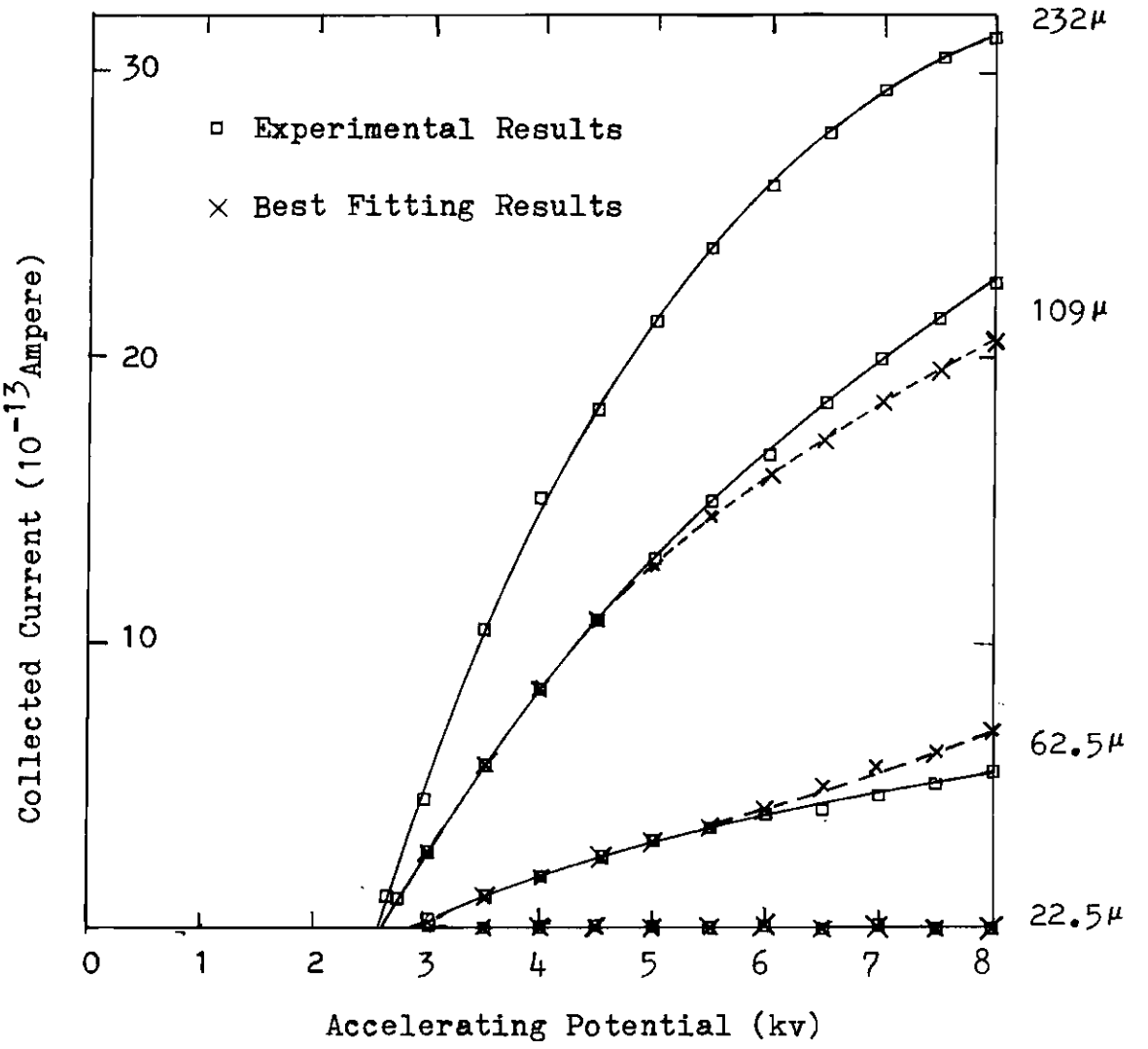

Figure 23. Best Fitting Curves for Persistence Current Measurements at 1.13°K for Different Nominal Grid Sizes

current through the 232-μ grid is taken as the standard current I_1. The onset potentials are slightly different because temperatures were not quite the same as the measurements were taken on different days. Corrections have been made as we fitted the best value for the size of the persistence ion complex by shifting the curves to the same onset potential and then back to their original positions after the fitting had been made. Detailed fitting procedures are discussed in Appendix II. Dashed lines in Figure 23 represent the fitting results while the solid lines are the experimental results. Fitted and experimental results are both zero for the 22.5-μ grid. Figures 24 and 25 are similar results at temperatures of 1.17°K and 1.21°K. In the present analysis, only one parameter, the diameter of the persistence ion complex, is involved. The fit is fairly good although not perfect. Assuming that the interaction between persistence ion complexes and grids is not perfectly geometric, or assuming that more than one ion size is involved would introduce more parameters and allow a better fit. Our data are not sufficient to uniquely determine more than one parameter.

Noise in the measurements was about 1×10^{-13} ampere for large currents ($\sim 10^{-11}$ ampere) and reduced to 0.3×10^{-13} ampere for small currents ($\sim 10^{-13}$ ampere).

Temperature Dependence of Onset Potentials

The onset potential for the persistence ion complex is temperature dependent. Higher temperature requires larger accelerating electric potential to start persistence currents. Figure 26 shows the

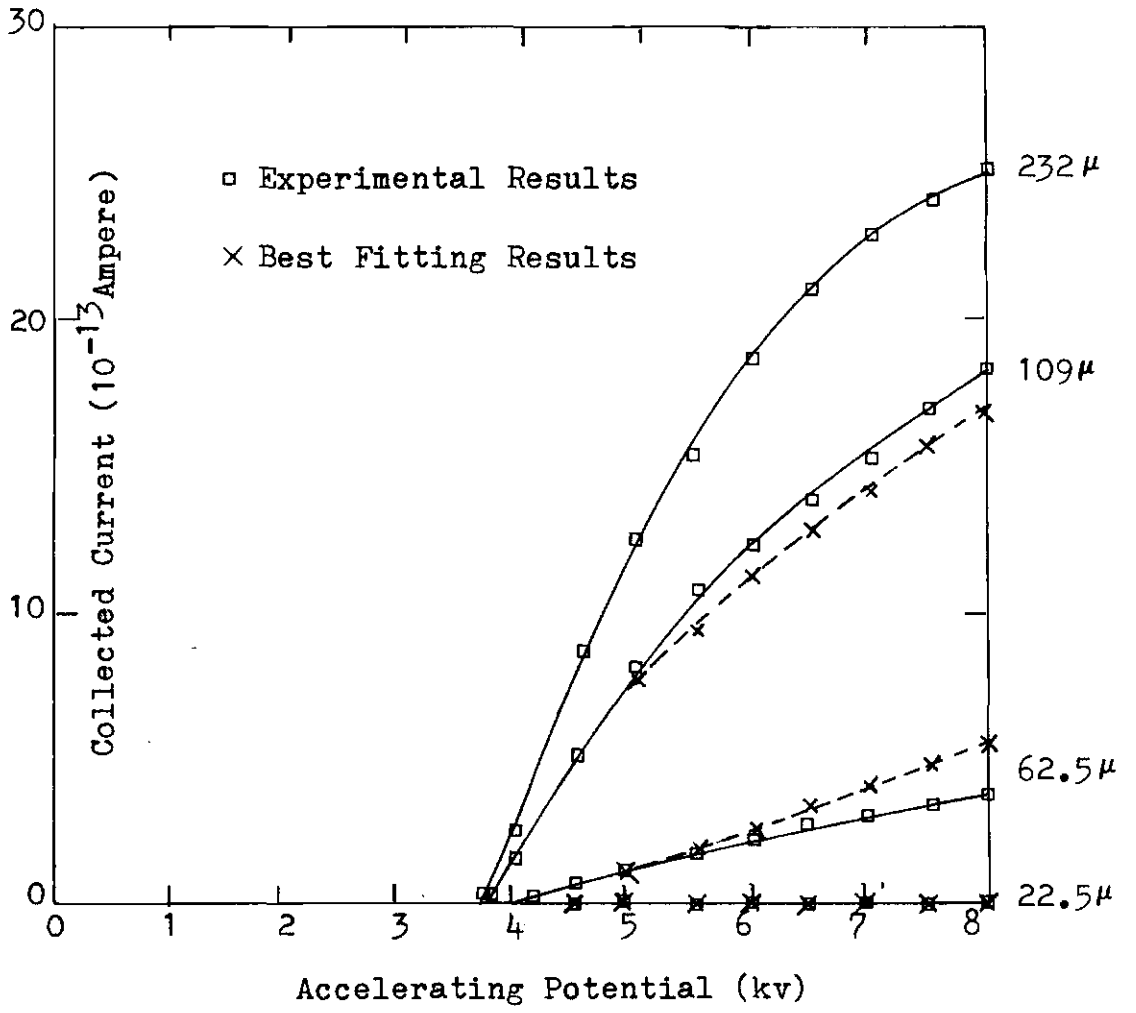

Figure 24. Best Fitting Curves for Persistence Current Measurements at 1.17°K

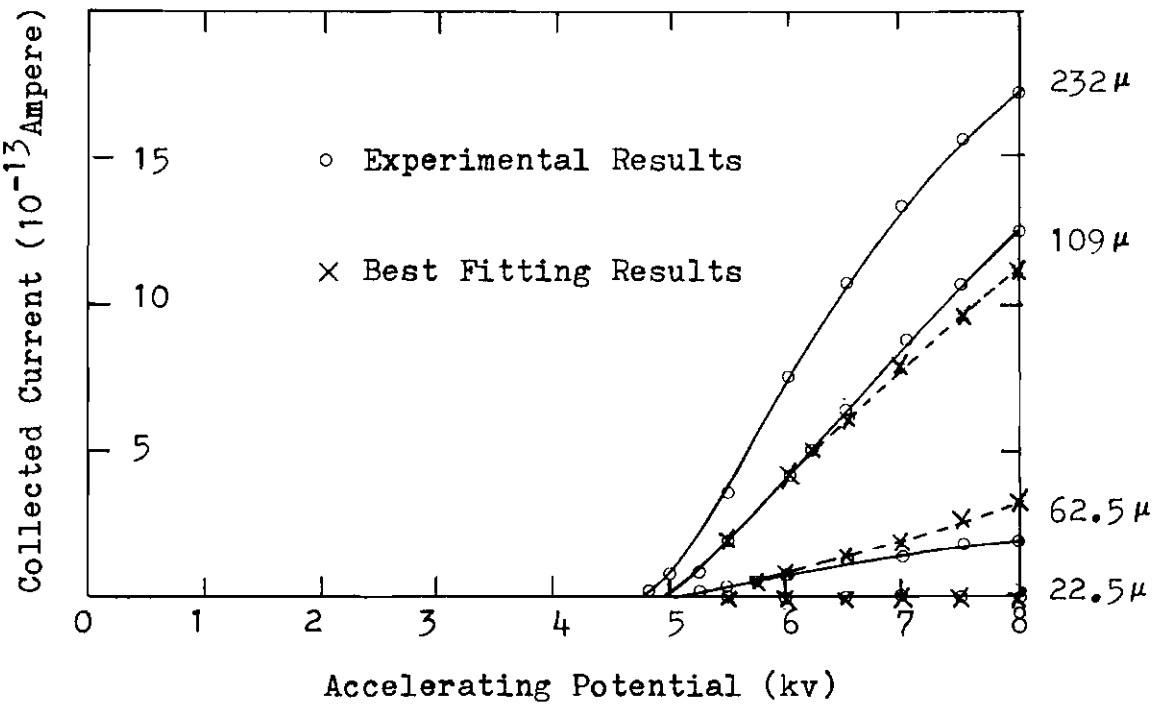

Figure 25. Best Fitting Curves for Persistence Current Measurements at 1.21°K

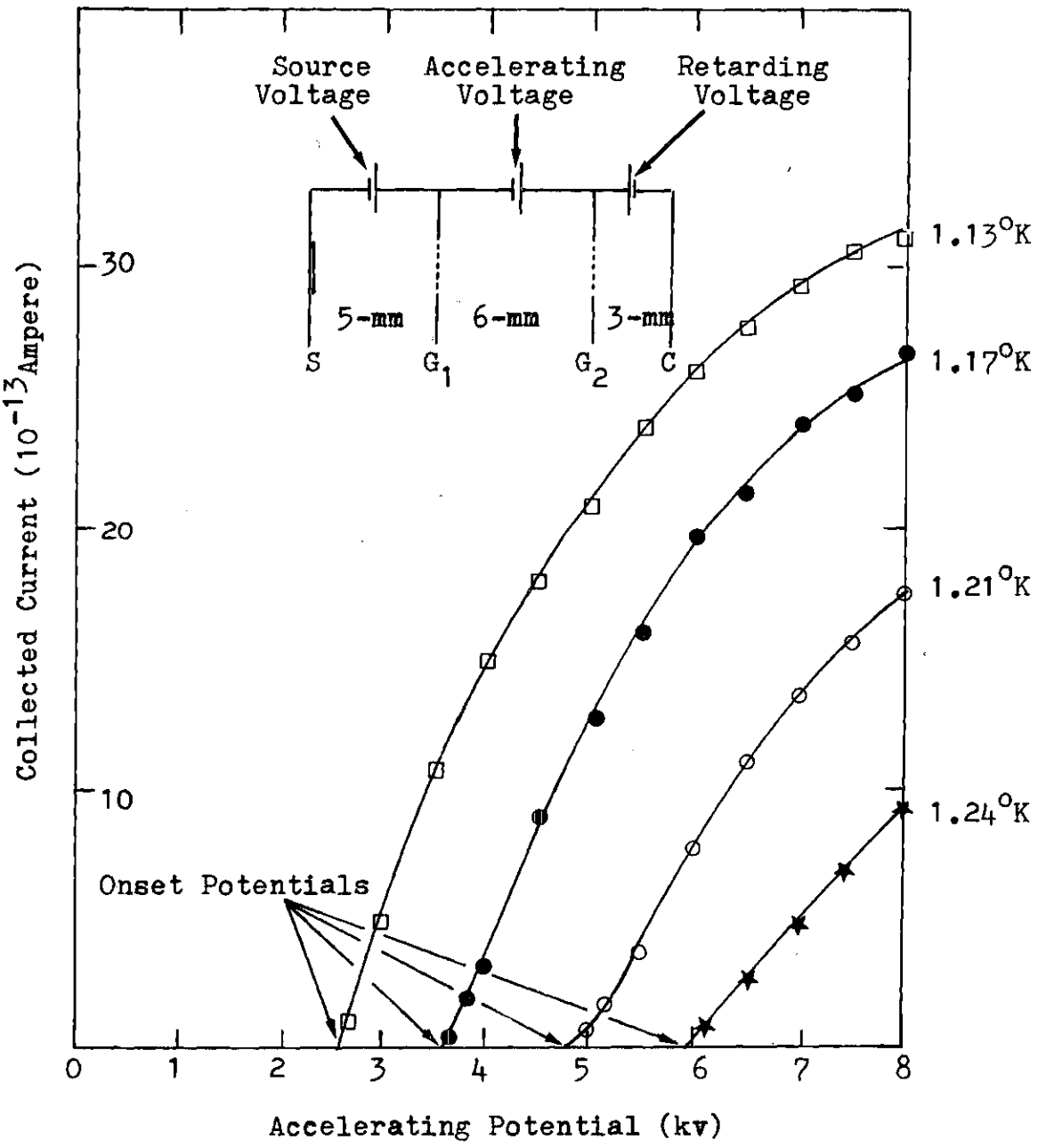

Figure 26. Persistence Currents for 232-μ Grid at Various Temperatures

onset potentials for a 232-μ grid at four different temperatures. In Figure 27, the temperature dependent onset field of the persistence current is plotted against the reciprocal of the absolute temperature on a logarithmic scale. Circles represent BMM's results, while the four stars indicate the onset field of our persistence ion complex at the temperatures of 1.13°K, 1.17°K, 1.21°K and 1.24°K. The onset field of our persistence ion complex is in good agreement with BMM's onset field of second sound attenuation.

Even Field Measurements

A second kind of measurement intended to monitor the total current was made by applying a collecting electric potential between the second grid and the collector. The electric field there was arranged to be equal to the electric field between the first and the second grids. Thus, the electric field was uniform all the way from the first grid to the collector. The second grid served only as a barrier, it had no effect on the acceleration of the persistence ions. Figure 28 shows these "even field" measurements for various sizes of grids at the temperature of 1.13°K, while Figure 29 indicates similar results for the 232-μ grid at four different temperatures. Each even field curve has a sharp discontinuity in slope at the persistence onset potential. The discontinuity is clear even for the 22.5-μ grid, although no current was collected for the 22.5-μ grid in the size measurements. (See Figure 20). These two measurements indicate that the persistence ion complex reaches the second grid but is unable to pass through the grid without losing its persistence property when its

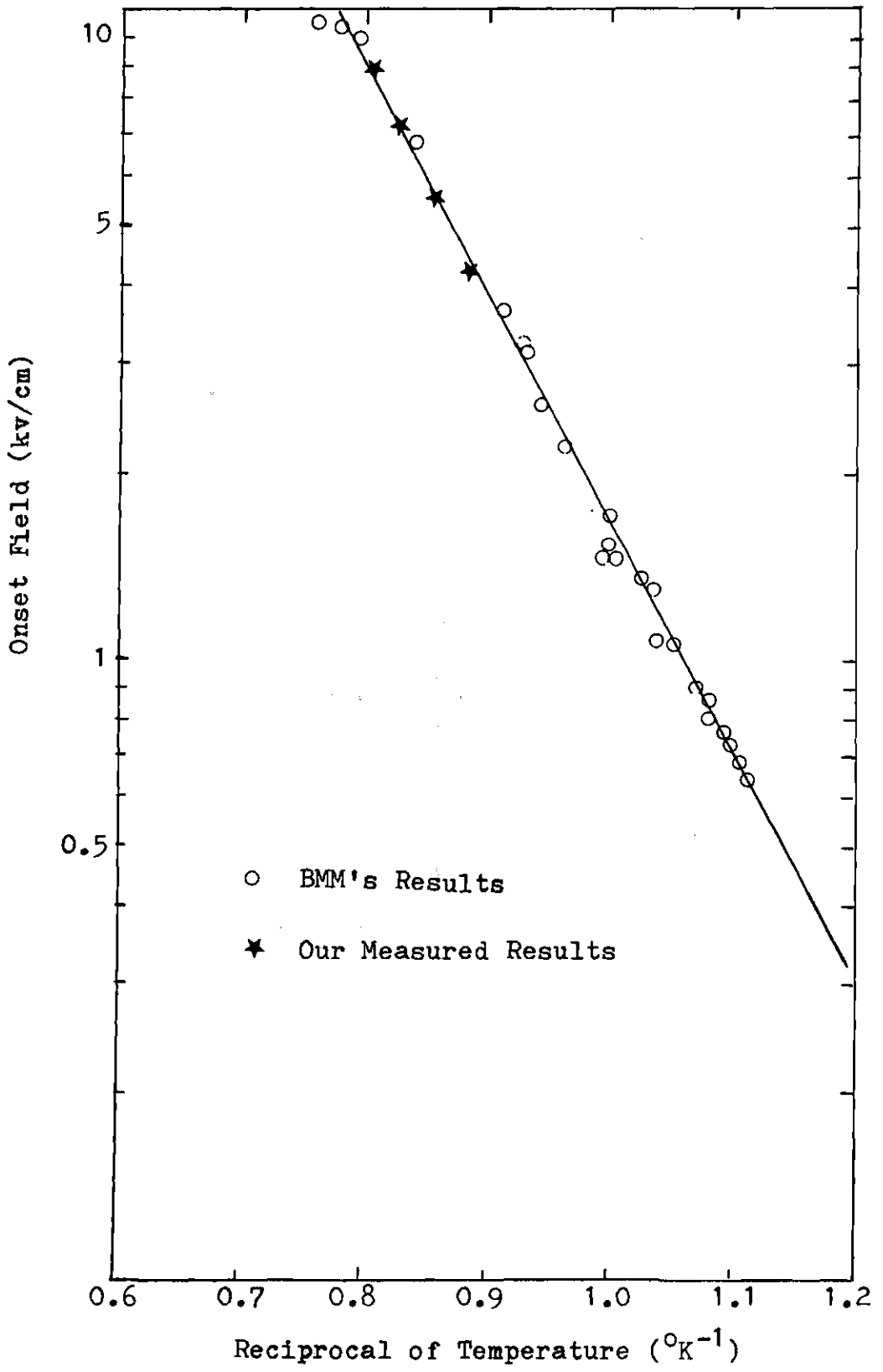

Figure 27. Onset Field vs Reciprocal of Temperature

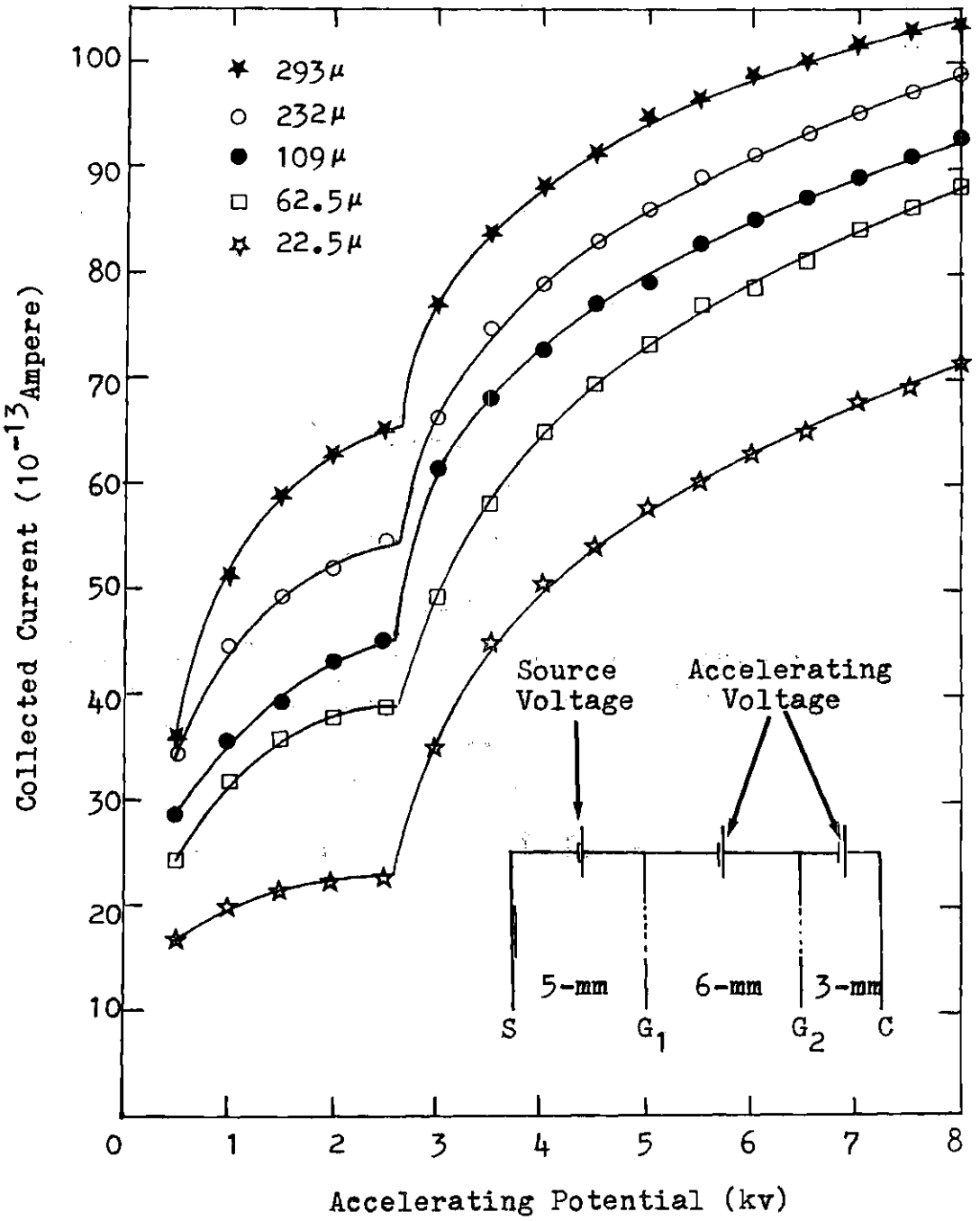

Figure 28. Even Field Currents for Different Sized Grids at 1.13°K

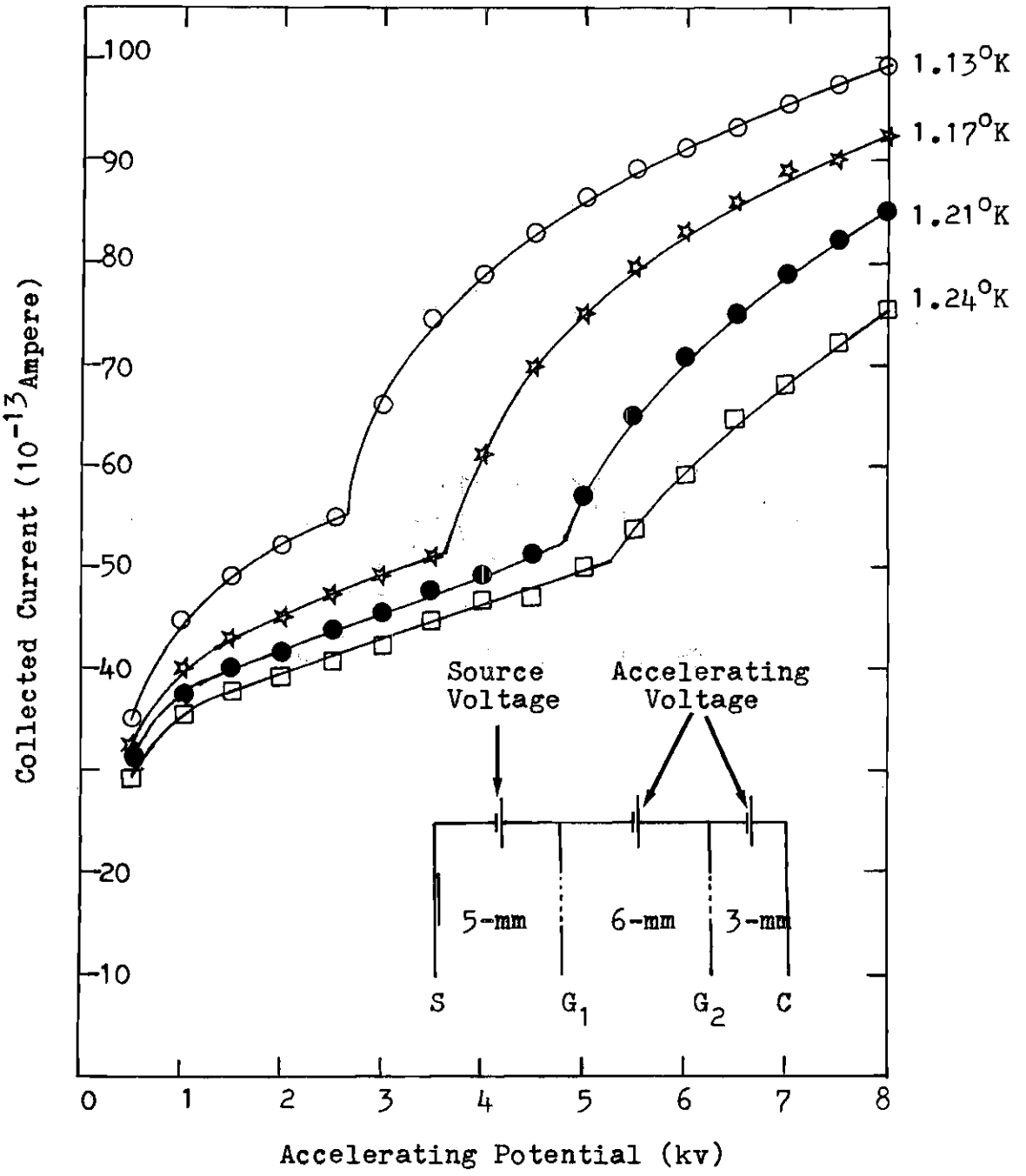

Figure 29. Even Field Currents for 232-μ Grid at Various Temperatures

size is larger than the grid opening. The ion complex breaks up as it hits the grid wire. After breaking up, the bare ion is attracted to the collector by the attractive field in the even field measurements, but it can not overcome the retarding potential in the size measurements. The difference in magnitude of the curves in Figure 28 is primarily due to differences in transmissions of the various grids.

There are two possible reasons for the discontinuity at the onset potential. One is that the ion beam may become more collimated causing more ions to reach the grid. The other possibility is that a larger proportion of the ion may pass through the grid. In order to distinguish between these two possibilities, we first examined how well the ion beam was collimated as it reached the grid. The current passing through the 0.125-inch diameter exposed area of the grid and the current stopped by the phosphor bronze plate which the grid was welded on were measured separately. The results indicated that 99.5 percent of the ion passed through the 0.125-inch diameter exposed area of the grid. This fact ruled out the possibility that the discontinuity was due to an ion beam spreading effect. We then examine the possibility that more of the ions passed through the grid when the accelerating potential was larger than the onset potential. In order to measure the amount of current reaching the 0.125-inch diameter exposed area, the second grid was replaced by a plate with a 0.125-inch diameter hole at the center (no grid mesh on it). The measured results showed a smooth curve all the way from low potential to high potential as indicated by Curve (A) of Figure 30, no discontinuity in slope was found at the onset potential. Curve (B) represents the even field

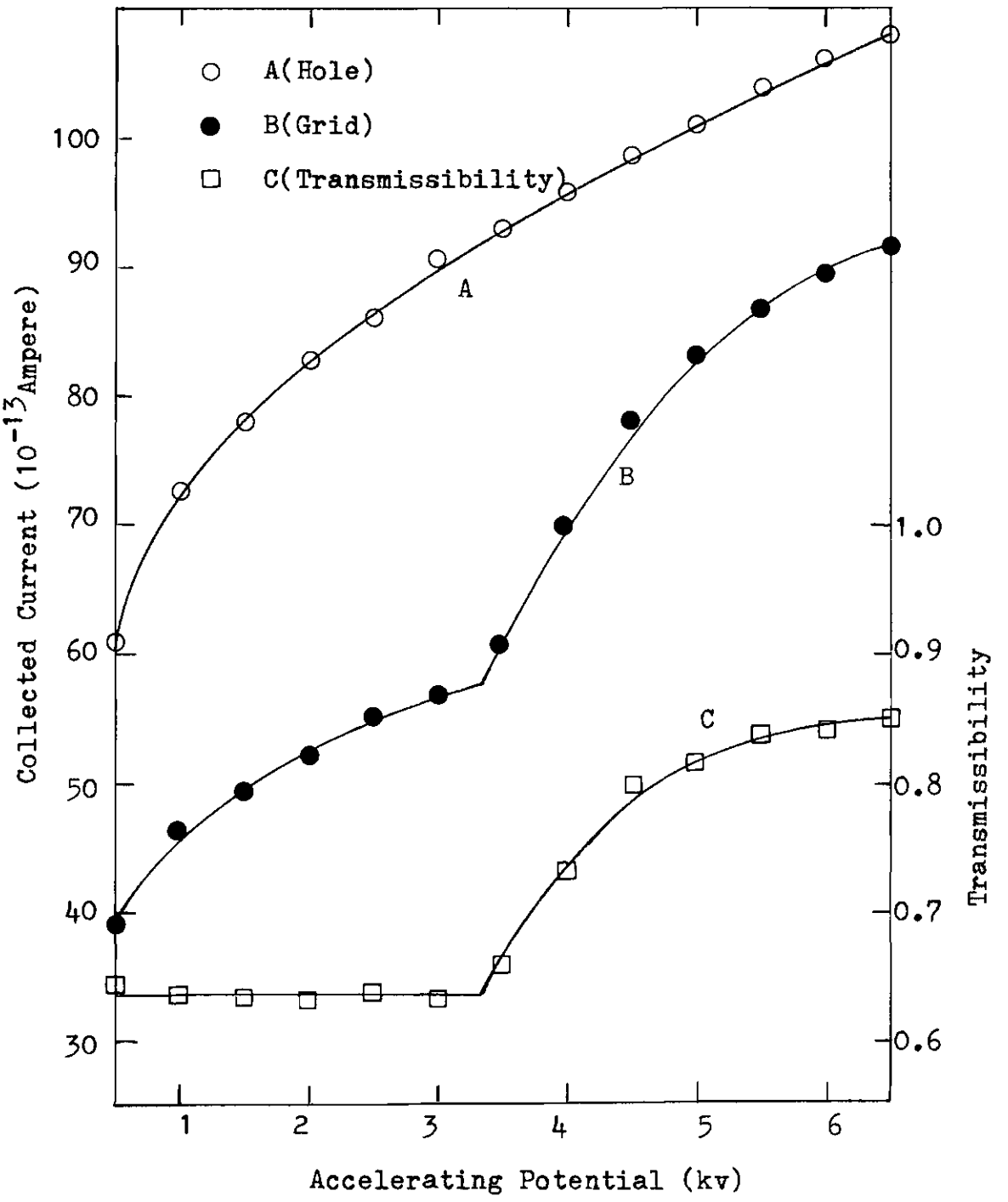

Figure 30. Transmissibility of 293-μ Grid at 1.17°K

measurements for a 293-μ grid at the same temperature (1.17°K). At each potential, the ratio of the amount of current passing through the grid to the amount of current reaching the grid (the amount of current passing through the hole) is plotted as Curve (C). We named this ratio the "transmissibility" of that grid. The transmissibilities of a 293-μ grid at four different temperatures are plotted in Figure 31. The results indicate that the transmissibility is almost field and temperature independent before the persistence ion complex is created, a larger proportion of current passes through the grid above the onset potential, and the current reaches a limit at high electric potentials.

Very High Field Behavior

The high electric potential that can be used to accelerate the ions is limited to 8,000 volts by our power supply. In order to investigate the behavior of the persistence ion complex at very high electric fields, we reduced the distance between the two grids from 6-mm to 3-mm and the distance between the second grid and the collector from 3-mm to 1.5-mm. Persistence current and even field measurements were made with this new arrangement. In the persistence measurements, a 5-volt retarding potential was applied across the 1.5-mm space between the second grid and the collector. It was found that persistence currents vanished at sufficiently high electric potentials, as indicated in Figure 32. Similar current reductions were observed in the even field measurements, as shown in Figure 33. The second grid used in these measurements was 293 microns, hence the reduction of the current was not a grid

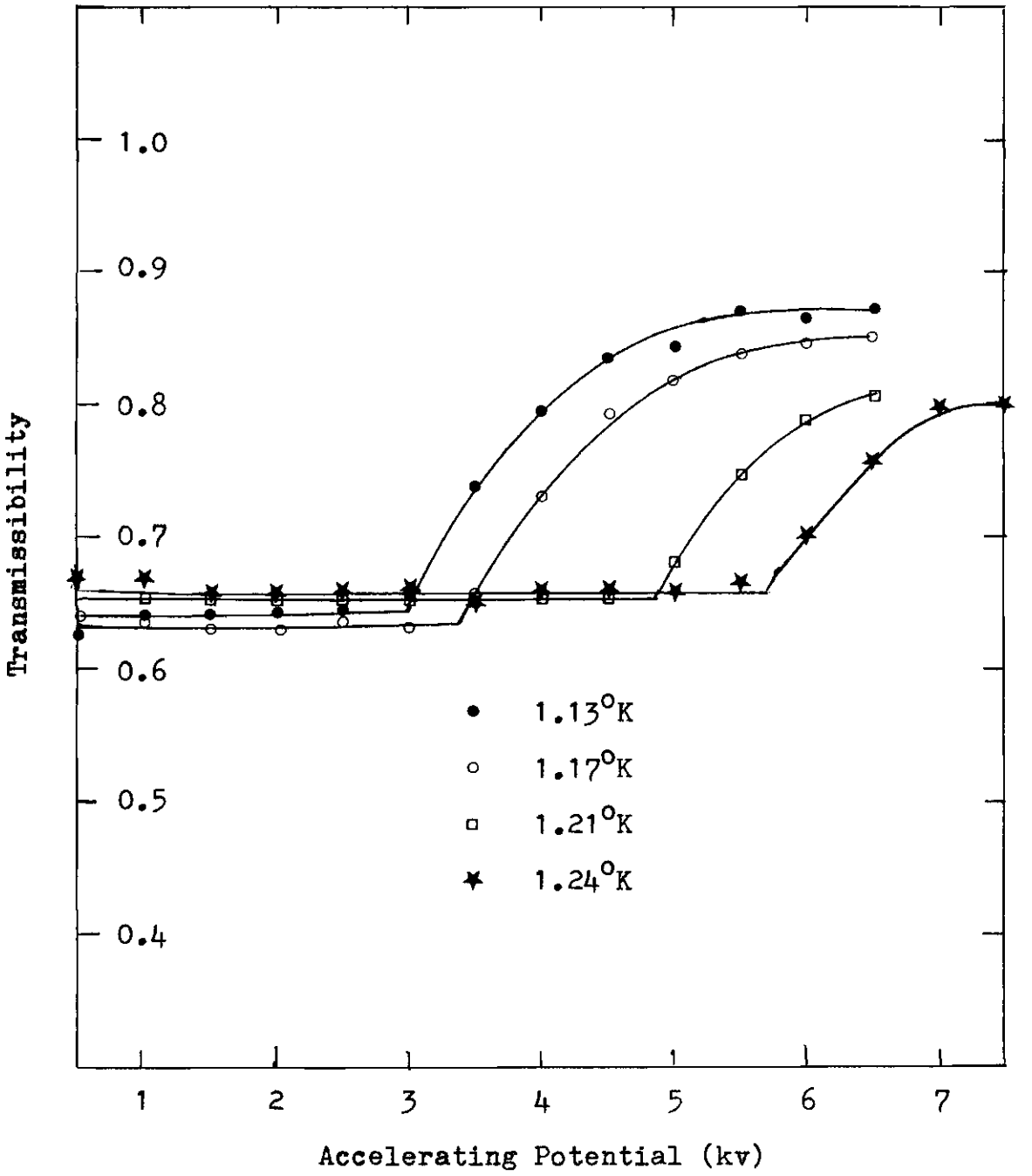

Figure 31. Transmissibility of 293-μ Grid at Various Temperatures

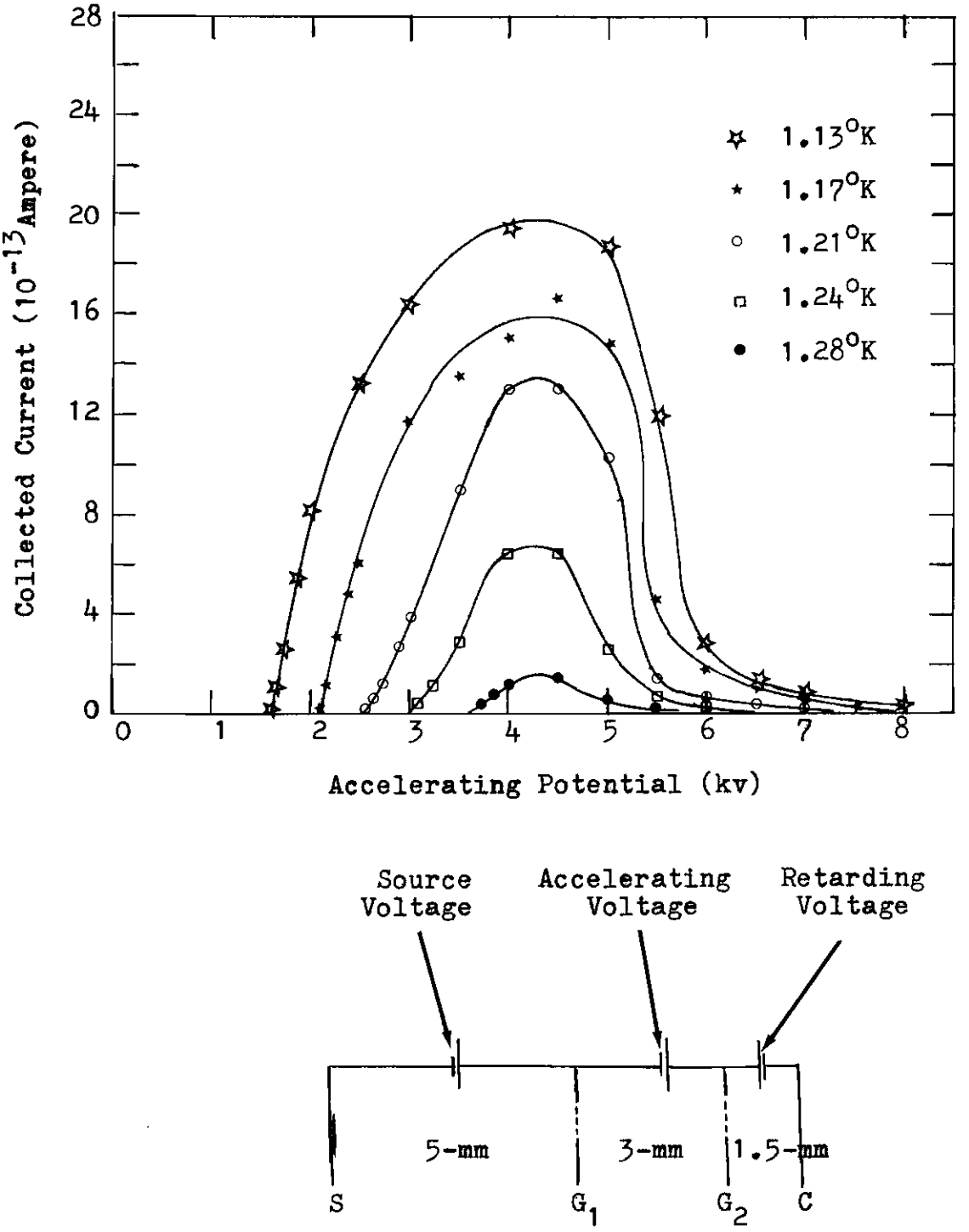

Figure 32. High Field Behavior of Persistence Current

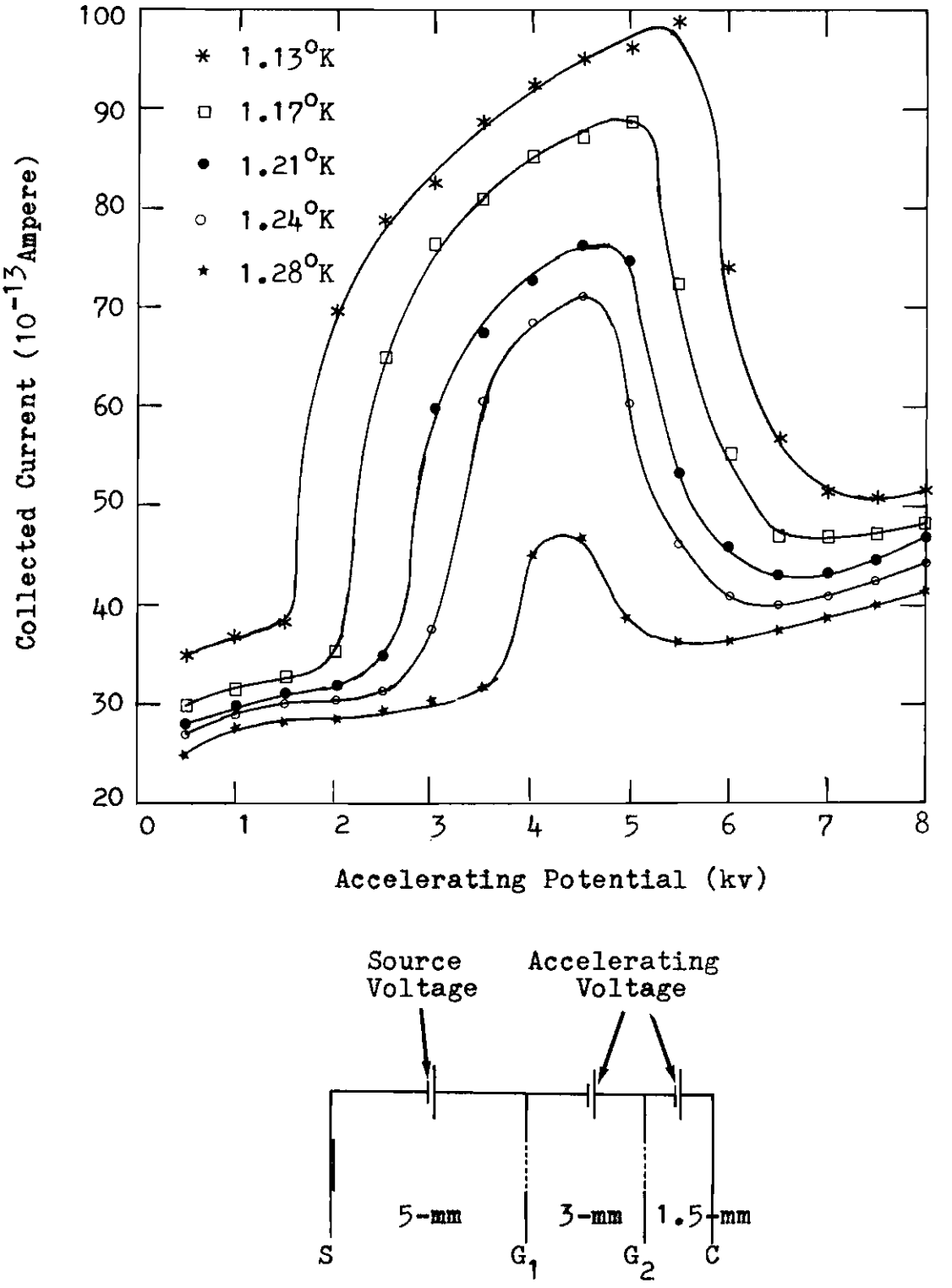

Figure 33. Even-Field Measurements at High Electric Fields

size effect. It could be due to the escape of ions from the dydrodynamic persistence ion complexes. The energy of the escaped ions would be too small to allow them to overcome the retarding potential and reach the collector. It is well known that positive ions escape from vortex rings at high electric fields.[11,25] If the persistence ion complex is some kind of complex involving vortex cores (as seems likely), our results would be the first observations that negative ions escape from vortex cores at very high electric fields.

Persistence Creation Conditions

In the previous measurements, the electric potential between the source and the first grid was kept at 400 volts which was smaller than the critical potential necessary to create a vortex ring. This means that the ions were still in the bare ion state as they passed through the first grid. They were then accelerated from the first grid to the second grid. The persistence ion complex is created in this accelerating region. It is not clear whether the ions transform directly into persistence ion complexes or whether they first form vortex rings and then transform into persistence ion complexes. The following experiment has been done to examine this problem.

An electric potential which is large enough to create vortex rings but too small to create persistence complexes was applied between the source and the first grid. This means that ions were in the vortex ring state as they passed through the first grid. The result of this experiment is that persistence ion complexes began to be observed at the same potential as in our other measurements. This proves that

the persistence ion complex can be created from an ion in a vortex ring. It does not rule out the possibility that the persistence ion complex could also be created from a bare ion.

Experimental Defect Analyses

It is always possible that the measured results consist of some experimental defects. The following measurements have been made to clear up these possibilities.

1. Various potentials have been applied between the source and the first grid. The results, indicated in Figure 34, show only a change in magnitude in the collected currents. The shape of the curves are similar and the onset potentials fall at the same potential. This indicates that the magnitude of the collected current is controlled by the source potential. This proves that the measured currents originate at the radioactive source.

2. The fact that the collected current can be stopped by reducing the grid size proves that the collected currents pass through the grids not through other conducting objects.

3. In order to be sure that the large accelerating electric field did not reach the collector, an additional grid was used to shield the collector. The second and the third grids were shorted together and separated by a distance of 6-mm, so that the persistence ion complex had to cross a 6-mm field free region after it had been accelerated and before it entered the small retarding field region. Persistence currents were still observed.

4. Measurements were also made by reversing all of the potentials.

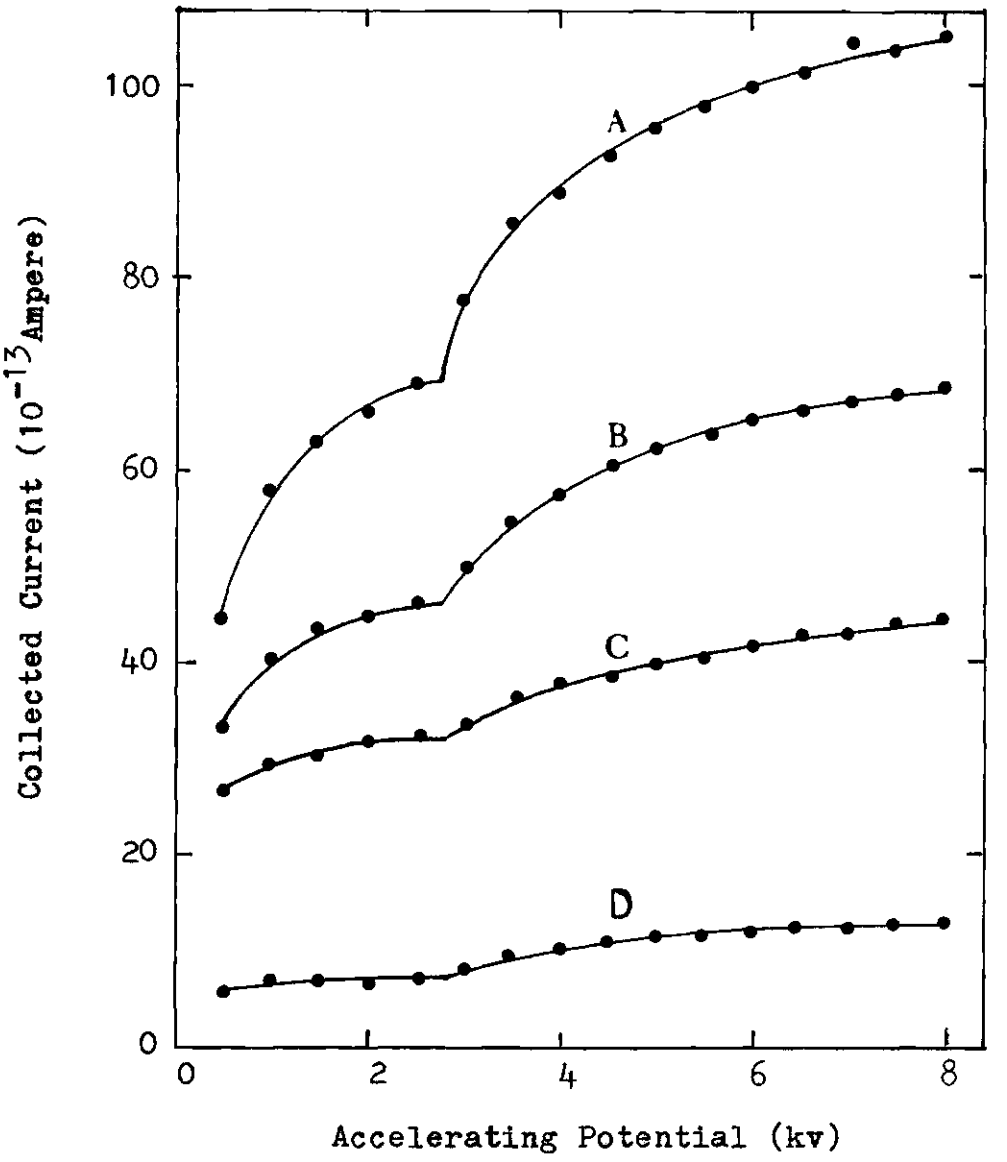

A: 400-volt Source Potential
B: 210-volt Source Potential
C: 110-volt Source Potential
D: 34-volt Source Potential

Figure 34. Even-Field Measurements for Different Source Potential at 1.13°K

The fact that no current was collected indicated that the large potential did not produce any false effects.

The above examinations seem to indicate that the measured ion currents originate at the radioactive source and pass through the liquid helium and grids to reach the collector. In addition to these examinations, we have compared our measurements with BMM's results. It seems unlikely that experimental defects were involved in our observations.

CHAPTER IV

DISCUSSIONS AND CONCLUSIONS

Comparison Between the Persistence Ion Complex and the Fast Ion

In 1969, Doake and Gribbon[47] reported evidence of finding a new state of the negative ion in liquid helium. They named this kind of ion the "fast ion". Their discovery was later (1971) confirmed by Ihas and Sanders.[48] Our persistence ion complex and Doake and Gribbon's fast ion have several things in common. (1) The nature of both are unknown. (2) They both are related to vortex rings. (3) Doake and Gribbon observed the fast ions at the same temperatures as BMM had observed the persistence currents. Both had current increase at comparable electric fields. (4) Both had size effects. Therefore it is natural to connect the fast ion and our persistence ion complex together. However, after more extensive comparison between them, several discrepancies have been found. Detailed discussions are presented as follows:

1. Authors of both papers have reported that the fast ion velocity had a linear dependence on the electric field at low fields and reached a limiting value at high fields. They also found that the velocity of the fast ion only depended on the field at which it was measured and not on the field at which it was created. This fact indicates that the fast ion is in equilibrium with the electric field.

As for the persistence ion complex, the fact that it has non-zero velocity in zero field or retarding field regions indicates that the persistence ion complex is not in equilibrium with the electric field.

2. Doake and Gribbon observed that the fast ion was created at the critical field necessary to create vortex rings, that is, at E_{c1} of Figure 1. On the other hand, the persistence ion complex is created at a field near E_{c2} which is higher than E_{c1}.

3. Doake and Gribbon measured the drift velocity of the fast ion by using the Cunsolo method.[49] This method is accurate only for measuring low energy ions.[10] Ihas and Sanders used a time-of-flight method, which is accurate for ions of all energies, to measure the drift velocity of the fast ion and they obtained the same results as Doake and Gribbon. From these two facts, it can be concluded that the fast ion is a kind of low energy particle. As for the persistence ion complex, our observations show that it is very energetic from its ability to overcome a large retarding potential. Since there is some difficulty in transferring charge from the persistence ion complex to the collector if the retarding field at the collector is too large, a third grid has been placed between the second grid and the collector. A small collecting potential was applied across the 3-mm distance between the third grid and the collector while a large retarding potential was applied across the 3-mm distance between the second and the third grids. With this arrangement, if the ion could overcome the large retarding field, it would easily be collected. The ion had to have large energy to overcome the large retarding field. The results showed that the persistence ion complex had been collected even at a

retarding potential of 4,000 volts.

4. Doake and Gribbon's constant collecting field curves and our even field curves have one common nature, that is, attractive fields are applied at the collector in both cases. The current characteristics should be similar if the persistence ion complex and the fast ion are the same kind of particles. However, after comparing Doake and Gribbon's results (Figure 35) and our even field results (Figure 33), several significant differences have been found between the two sets of current characteristics. (A) Doake and Gribbon's current increases to a plateau at small fields and then a sharp increase starts at the critical field for vortex ring creation. The current peak appears at the critical field for the persistence creation. The current at the peak has a magnitude about five to ten times larger than the plateau current. As for our persistence ion complex, the even field curve has a sharp increase starting at the critical field for persistence current creation. Instead of a sharp peak, our curve has a broad hump at fields higher than the cirtical field for persistence current creation. (B) Doake and Gribbon's current peak was undetectable for temperatures higher than $1.02^{\circ}K$, while all of our measurements were made at temperatures at or above $1.13^{\circ}K$. A broad hump existed in all measurements.

5. The size effects of grids are different too. Doake and Gribbon's current peak appeared for relatively smaller sizes of grid spaces and vanished for larger grid spaces,[50] as shown in Figure 36. Our even field currents were measurable for all sizes of grids and they all had broad humps at high fields. In our retarding field measurements,

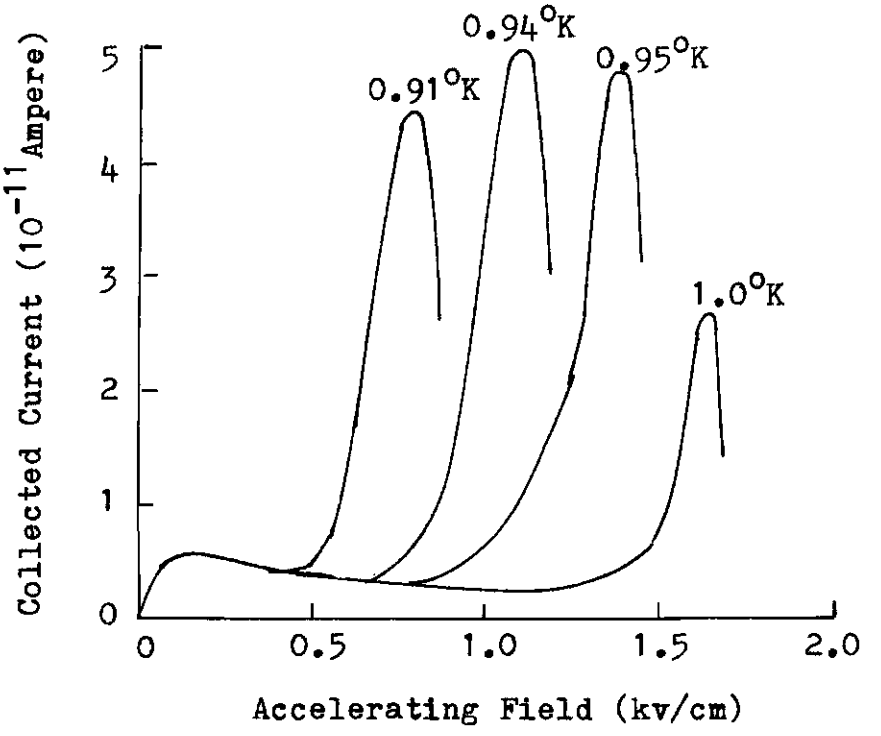

Figure 35. Doake and Gribbon's Fast Ion Measurements at Various Temperatures

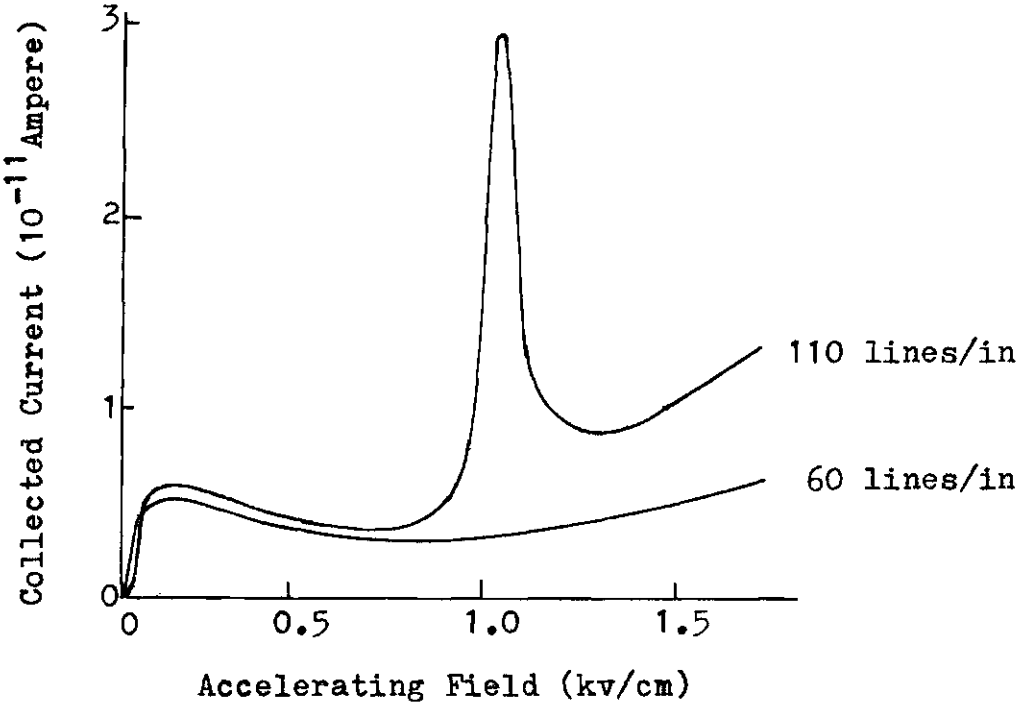

Figure 36. Size Effect of the Fast Ion (After Doake and Gribbon)

the current was present for larger sizes of grid spaces and absent for smaller sizes of grids.

From the above discussions, it seems likely that the physical origins of the persistence ion complex and the fast ion are different.

Creation of Persistence Ion Complex

From our experimental observations which we discussed in Chapter III, it is understood that ions are in the vortex ring state immediately before the formation of the persistence ion complexes. It is of great interest to examine how a vortex ring transforms into a persistence ion complex. There are two possible kinds of transformations. One is a direct transformation from a vortex ring to a persistence ion complex, and the other, the trapped ion escapes from the vortex ring and then creates a persistence ion comples. If an ion escapes from a vortex ring, it will in general immediately form a new vortex ring. Since the old and the new rings are close to each other, there is a possibility that the two singly quantized vortex rings may combine together to create a doubly quantized vortex ring. The doubly quantized vortex ring has different core structure from the singly quantized vortex ring. The ion escape probability from a double quantized vortex ring might be smaller than that from a singly quantized vortex ring. In Chapter I, we have the energy and the circulation of a vortex ring as

$$\epsilon = \tfrac{1}{2}\,\rho\kappa^2 r(\ln - 7/4). \tag{7}$$

and

$$\kappa = Nh/m. \tag{25}$$

where $\eta = \ln(8r/a)$. Substituting equation (25) into equation (7), yields

$$\epsilon = \tfrac{1}{2}\,\rho(\eta - 7/4)(h/m)^2\, rN^2 \ . \qquad (26)$$

Since $r \gg a$, the parameter η is a insensitive function of r, so that equation (26) can be reduced to

$$r \approx C\,\frac{E}{N^2} \ . \qquad (27)$$

where C is a constant.

From equation (27), it is clear that the size of a doubly quantized vortex ring is only one-forth of the size of a singly quantized vortex ring if they have the same amount of energy. Therefore the diameter of a doubly quantized vortex ring with an energy of 4,000 eV is 32 microns (one-fourth of 130 microns, the diameter of a singly quantized vortex ring with the same energy). This value is about what we have measured. This small ring size will tend to reduce the frictional force although a recent theoretical work[51] indicates that the force per unit length of such a ring is probably larger than that of a normal ring. The size of such a ring ought to increase with the electric field. However, as indicated in Figure 22, our calculations indicate that the size of the persistence ion complex is almost field independent. It is not certain that this explanation should be excluded because the situation might be complicated by occasional ion escapes. However, this is a serious objection to this explanation. All models of persistence current which depend on ion escapes from vortex rings have one common objection, the onset field

for the persistence ion complex increases with temperature, contrary to the well known electric field and temperature dependence of positive ions escaping from vortex rings. Therefore we favor the view-point that persistence ion complexes are transformed from vortex rings.

Vortex rings can be deformed by unsymmetric forces. According to our calculation, a vortex ring at the persistence onset potential has a radius of about 0.1 micron. As an ion drifts around such a large ring, the electric field force which acts on the ion only, acts on the vortex ring unsymmetrically. Such an unsymmetric force could cause the vortex ring to deform. One possible results from this deformation would be an ion attached to a tangled vortex core. The possibility that this complex might have a reduced frictional force should be considered although it is not obvious. It is also possible that a doubly quantized vortex ring is created through such a deformation. BMM's second sound attenuation results seem to support a vortex model.

Conclusions and Recommendations

Difficulties appear in all the models we have considered. In order to understand entirely the characteristics of the persistence ion complex, more theoretical analysis and experimental investigation are needed. Among them, time-of-flight measurements would be most helpful. Bruschi and Santini[10] measured the velocity of the ion beam in collecting electric fields by an indirect method. If the ion beam is a kind of mixture of vortex rings and persistence ion complexes, their technique could easily miss the persistence ion complexes and measure only the vortex rings. What is needed is a measurement of the

velocity of the ion beam with a direct technique under conditions insuring that ions are in the persistence ion complex state. This nature can be determined by allowing the ion beam to pass through a retarding electric field. It is also necessary to make more theoretical analyses to find a possible model fitting the persistence ion complex.

APPENDIX I

SIZE COMPUTATION OF PERSISTENCE ION COMPLEX

In Figures 23, 24 and 25, our measured persistence currents for various grid sizes at three different temperatures were plotted against the applied electric potentials.

The purpose of this chapter is to discuss in some detail the procedures used in finding the best fitting values for the sizes of the persistence ion complexes. Equation (22) gives the amount of current passing through a particular size of grid as

$$I_x = I_o T_x((L_x-D)/L_x) \quad . \tag{28}$$

If the amount of current I_a passing through a grid of size L_a is known, then the amount of current I_b passing through a grid of size L_b can be easily computed by comparing the ratio of these two currents.

$$I_b = (T_b/T_a)((L_b-D)/(L_a-D))(L_a/L_b)I_a \quad . \tag{29}$$

If the measured currents of three or more different sizes of grids are known, the size of the persistence ion complex can be determined by keeping the measured current of one grid size as a standard and using a particular value for the size of the persistence ion complex which is the best value to fit the currents passing through all other sizes of grids. For example, at a temperature of 1.13^{o}K and an applied electric potential of 7,500 volts, the measured currents for four sizes

(232,109, 62.5 and 22.5 microns) of grids are

$$I_{232} = 30.5 \times 10^{-13} \text{ ampere.}$$

$$I_{109} = 21.3 \times 10^{-13} \text{ ampere.}$$

$$I_{62.5} = 5.10 \times 10^{-13} \text{ ampere.}$$

$$I_{22.5} = 0.$$

The ratios of transmissions are

$$T_{109}/T_{232} = 0.950, \quad T_{62.5}/T_{232} = 0.798.$$

The next step is to pick a particular value for D to fit the above four currents. For example, let D be 30 microns, then, from equation (29), the computed currents for the 109-μ and 62.5-μ grids with the 232-μ grid as a standard are

$$I'_{109} = 20.0 \times 10^{-13} \text{ ampere.}$$

$$I'_{62.5} = 8.66 \times 10^{-13} \text{ ampere.}$$

Then the deviations in currents are

$$\Delta I_{109} = I'_{109} - I_{109} = -1.3 \times 10^{-13} \text{ ampere.}$$

$$\Delta I_{62.5} = I'_{62.5} - I_{62.5} = 3.6 \times 10^{-13} \text{ ampere.}$$

Several different values of D have been tried. Results are listed in Table 3.

Table 3. Best Fitting Values of Persistence Ion Complex Size with 7,500-volt Applied Electric Potential at 1.13°K.

$I_{109} = 21.3 \times 10^{-13}$ ampere.

$I_{62.5} = 5.1 \times 10^{-13}$ ampere.

D	I'_{109}	$I'_{62.5}$	ΔI_{109}	$\Delta I_{62.5}$
30	20.0	8.66	-1.3	3.6
31	19.9	8.20	-1.4	3.1
32	19.4	7.80	-1.9	2.7
33	19.1	7.40	-2.2	2.3
34	18.8	6.9	-2.5	1.8

Note: D is in microns.

All currents are in 10^{-13} ampere.

APPENDIX II

FITTING PROCEDURES

The best fitting values for the size of the persistence ion complex were chosen by making the deviations of currents for all sizes of grids the smallest. Lists of such deviations of the 109-μ and 62.5-μ grids for various applied electric potentials at three different temperatures are presented in Tables 4, 5 and 6. The computed results are plotted in Figures 23, 24 and 25.

Table 4. Minimum Deviations for Optimum Ion Size at 1.13°K

V	D	ΔI_{109}	$\Delta I_{62.5}$
8.0	31.0	-2.7	2.8
7.5	33.0	-2.2	2.3
7.0	34.5	-1.9	2.2
6.5	35.0	-1.6	1.7
6.0	36.5	-1.4	1.2
5.5	38.0	-0.8	0.9
5.0	38.5	-0.6	0.8
4.5	39.0	-0.5	0.5
4.0	41.0	-0.3	0.3
3.5	43.0	0.0	0.0

Note: V - Applied potentials in kv.

D - Size of persistence ion complex in micron.

ΔI's - Deviations of computed current in 10^{-13} ampere.

Table 5. Minimum Deviations for Optimum Ion Size at 1.17°K

V	D	ΔI_{109}	$\Delta I_{62.5}$
8.0	34.0	-2.2	2.2
7.5	35.0	-2.0	1.8
7.0	35.5	-1.5	1.7
6.5	36.0	-1.3	1.4
6.0	36.2	-1.1	1.2
5.5	37.0	-1.0	0.9
5.0	38.0	-0.4	0.7
4.5	39.0	-0.5	0.5

Note: Same as Table 4.

Table 6. Minimum Deviations for Optimum Ion Size at 1.21°K

V	D	ΔI_{109}	$\Delta I_{62.5}$
8.0	35.0	-1.9	1.8
7.5	36.0	-1.4	1.5
7.0	38.0	-1.1	1.0
6.5	40.0	-0.5	0.5
6.0	40.5	-0.2	0.2

Note: Same as Table 4.

BIBLIOGRAPHY

1. F. Reif and L. Meyer, Phys. Rev. 119, 1164 (1960).
2. R. L. Williams, Canadian J. Phys. 35, 134 (1953).
3. G. Careri, G. Scaramuzzi and J. O. Thomson, Nuovo Cimento, 13, 186 (1959).
4. J. Levins and T. M. Sanders, Phys. Rev. Lett. 8, 1959 (1962).
5. K. R. Atkins, Liquid Helium (Cambridge University Press, New York, 1959), p. 59.
6. G. W. Rayfield and F. Reif, Phys. Rev. Lett. 11, 305 (1963).
7. G. W. Rayfield and F. Reif, Phys. Rev. 136, 1194 (1964).
8. K. Schwarz, Phys. Rev. Lett. 24, 641 (1970).
9. G. Careri, S. Cunsolo and P. Mazzoldi, Phys. Rev. Lett. 7, 151 (1961).
10. L. Druschi and M. Santini, Rev. Sci. Inst. 41, 102 (1970).
11. L. Bruschi, P. Mazzoldi and M. Santini, Phys. Rev. Lett. 21, 1738 (1968).
12. R. J. Donnelly and P. H. Roberts, Proc. Roy. Soc. (London), A312, 519 (1969).
13. T. C. Padmore, Phys. Rev. A5, 356 (1972).
14. T. C. Padmore, Phys. Rev. Lett. 26, 63 (1971).
15. L. D. Landau, J. Phys. Moscow, 5, 71 (1941).
16. L. D. Landau, J. Phys. Moscow, 11, 91 (1947).
17. R. J. Donnelly and P. H. Roberts, Phys. Rev. Lett. 23, 1491 (1969).
18. L. Onsager, Nuovo Cimento, 6, Suppl. 2, 249 (1949).
19. R. P. Feynman, Progress in Low Temperature Physics, Vol. 1, pp. 34-53.

20. L. Prandtl and O. G. Tietjens, Fundamentals of Hydro- and Aeromechanics (Dover Publications, Inc., New York), pp. 209-212.

21. W. Thomson, Phil. Mag. (4), 38, 511 (1867).

22. Hicks. Phil. Trans. A, clxxvi, 756 (1885).

23. A. Gray, Phil. Mag. (6), 28, 13 (1914).

24. H. Lamb, Hydrodynamics (Dover Publications, New York, 1945), 6th ed., pp. 202-220.

25. A. G. Cade, Phys. Rev. Lett. 15, 238 (1965).

26. R. J. Donnelly, Experimental Superfluidity (University of Chicago Press, Chicago, Ill., 1967).

27. R. L. Douglass, Phys. Rev. Lett. 13, 791 (1964).

28. L. Bruschi, B. Maraviglia and P. Mazzoldi, Phys. Rev. 143, 84 (1966).

29. L. Tisza, J. Phys. Radium 1, 165, 350 (1940).

30. V. P. Peshkov, J. Phys. Moscow, 8, 131, 391 (1944).

31. Both dewars were purchased from the Labglass Inc., Vineland, New Jersey.

32. Hills McCanna Diaphragm Valve, Model 500, Hills-McCanna Co., Carpentersville, Ill.

33. Emerson & Cuming, Inc., Canton, Mass.

34. R. E. Little and Y. Liu, Rev. Sci. Inst. 44, 346 (1973).

35. Cary 401 Vibrating Reed Electrometer, Cary Instrument, Monrovia, Calif.

36. Grid meshes were purchased from the Buckbee Mears Co., St. Paul, Minn.

37. Atomex Immersion Gold Solution, Engelhard Industries, Inc. Newark, New Jersey.

38. Regulated High Voltage Power Supply, Universal Vortronics Corp., Mount Kisco, New York.

39. Harrison 6525A D.C. Power Supply, Hewlett Packard.

40. Instruction Manual, Cary 401 Vibrating Reed Electrometer, Cary Instruments, Monravia, Calif.

41. A. C. Rose-Innes, Low Temperature Techniques (The English University Press Ltd., London, 1964), p. 82.

42. G. K. White, Experimental Techniques in Low-Temperature Physics (Oxford at the Clarendon Press 1968), 2nd ed., p. 110.

43. The "1958 He^4 Scale of Temperatures", National Bureau of Standards, U. S. Dept. of Commerce.

44. Handbook of Mathematical Functions (U. S. GPO, Washington, D. C. 1966), edited by M. Abramowitz and I. A. Stegun, Chapt. 5.

45. G. Gamota and T. M. Sanders, Jr., Phys. Rev. A4, 1092 (1971).

46. G. Gamota and T. M. Sanders, Jr., Phys. Rev. Lett. 15, 949 (1965).

47. C. S. M. Doake and P. W. F. Gribbon, Phys. Lett. 30A, 251 (1969).

48. G. G. Ihas and T. M. Sanders, Jr., Phys. Rev. Lett. 27, 383 (1971).

49. S. Cunsolo, Nuovo Cimento, 21, 76 (1961).

50. C. S. M. Doake and P. W. F. Gribbon, J. Phys. C, Solid State Physics, 5, 2998 (1972).

51. M. Kuchnir, J. B. Ketterson and P. R. Roach, Phys. Rev. A6, 341 (1972).

VITA

Yu Liu was born in Shantung, China. He is the third son of Mr. and Mrs. W. K. Liu. He was married to Theresa Ning-ning Tsai. They have one child, Helen Chaonan Liu.

Mr. Liu received the degree of Bachelor of Science in Physics from Cheng Kung University and the degree of Master of Arts in Physics from Rice University.

Mr. Liu is a member of Sigma Pi Sigma.